TTP05-10
SFB/CPP-05-30
hep-ph/0507178

One-loop weak corrections to hadronic production of Z bosons at large transverse momenta

Johann H. Kühn[†], A. Kulesza[‡], S. Pozzorini[§], M. Schulze[¶]

Institut für Theoretische Teilchenphysik, Universität Karlsruhe
D-76128 Karlsruhe, Germany

Abstract:
To match the precision of present and future measurements of Z-boson production at hadron colliders, electroweak radiative corrections must be included in the theory predictions. In this paper we consider their effect on the transverse momentum ($p_{\rm T}$) distribution of Z bosons, with emphasis on large $p_{\rm T}$. We evaluate, analytically and numerically, the full one-loop corrections for the parton scattering reaction $q\bar{q} \to Zg$ and its crossed variants. In addition we derive compact approximate expressions which are valid in the high-energy region, where the weak corrections are strongly enhanced by logarithms of $\hat{s}/M_W^2$. These expressions include quadratic and single logarithms as well as those terms that are not logarithmically enhanced. This approximation, which confirms and extends earlier results obtained to next-to-leading logarithmic accuracy, permits to reproduce the exact one-loop corrections with high precision. Numerical results are presented for proton-proton and proton-antiproton collisions. The corrections are negative and their size increases with $p_{\rm T}$. For the Tevatron they amount up to -7% at 300 GeV. For the LHC, where transverse momenta of 2 TeV or more can be reached, corrections up to -40% are observed. We also include the dominant two-loop effects of up to 8% in our final LHC predictions.

July 2005

[†]Johann.Kuehn@physik.uni-karlsruhe.de
[‡]ania@particle.uni-karlsruhe.de
[§]pozzorin@particle.uni-karlsruhe.de
[¶]schulze@particle.uni-karlsruhe.de

1 Introduction

The study of gauge boson production has been among the primary goals of hadron colliders, starting with the discovery of the W and Z bosons more than two decades ago [1]. The investigation of the production dynamics, strictly predicted by the electroweak theory, constitutes one of the important tests of the Standard Model. Furthermore, this reaction contributes to the background for many signals of new physics. Being embedded in the environment of hadronic collisions, the reaction necessarily involves hadronic physics, like parton distributions, and depends on the strong coupling constant. In turn, the cross section for the production of W and Z bosons and their rapidity distribution can be used to gauge the parton distribution functions [2] which are important ingredients for the prediction of numerous reaction rates.

Differential distributions of gauge bosons, in rapidity as well as in transverse momentum (p_{T}), have always been the subject of theoretical and experimental studies. In the region of small p_{T}, multiple gluon emission plays an important role and contributions of arbitrary many gluons must be resummed to arrive at a reliable prediction [3, 4]. At larger transverse momenta the final state of the leading order process consists of a W or Z boson plus one recoiling jet. QCD corrections in next-to-leading order to this process are mandatory for the correct description and can amount to several tens of per cent depending on the observable under consideration, including jet definition, as well as the renormalization and factorization scales [5]. The evaluation of next-to-next-to-leading order corrections involves two-loop virtual plus a variety of combined virtual plus real corrections and is a topic presently pursued by various groups (see e.g. Ref. [6]).

For the experiments at the Large Hadron Collider (LHC) a new aspect comes into play. The high center-of-mass energy in combination with the enormous luminosity will allow to explore parton-parton scattering up to energies of several TeV and correspondingly production of gauge bosons with transverse momenta up to 2 TeV or even beyond. In this region electroweak corrections from virtual weak boson exchange increase strongly, with the dominant terms in L-loop approximation being leading logarithms of the form $\alpha^L \log^{2L}(\hat{s}/M_W^2)$, next-to-leading logarithms of the form $\alpha^L \log^{2L-1}(\hat{s}/M_W^2)$, and so on. These corrections, also known as electroweak Sudakov logarithms, may well amount to several tens of percent. They have been studied in great detail for processes involving fermions in Refs. [7, 8]. Investigations on the dominant and the next-to-leading logarithmic terms are also available for reactions involving gauge and Higgs bosons [9, 10, 11]. A recent survey of the literature on logarithmic electroweak corrections can be found in Ref. [12]. The impact of these corrections at hadron colliders has been studied in Ref. [13]. Specifically, hadronic Z-boson production at large p_{T} has been investigated in next-to-leading logarithmic approximation, including the two-loop terms [14]. Numerical results for the complete one-loop terms have been presented in Ref. [15].

It is the aim of this work to obtain an independent evaluation of the complete

one-loop weak corrections to the same reaction, and to present the full result in analytic form. At the partonic level the reactions $q\bar{q} \to \mathrm{Z}g$, $qg \to \mathrm{Z}q$ and $\bar{q}g \to \mathrm{Z}\bar{q}$ with $q = u, d, s, c$ or b have to be considered which are, however, trivially related by crossing and appropriate exchange of coupling constants. We split the corrections into an "Abelian" and a "non-Abelian" component. The ultraviolet divergences of the former are removed by the renormalization of the fermion wave functions as expected in Abelian theories. The latter receives also divergent contributions from the renormalization of the Z-boson wave function and the electroweak parameters. The electroweak coupling constants are renormalized in the framework of the modified minimal subtraction ($\overline{\mathrm{MS}}$) scheme. We present analytic results for the exact one-loop corrections that permit to predict separately the various quark-helicity contributions. We also derive compact analytic expressions for the high-energy behaviour of the corrections. Here we include quadratic and linear logarithms as well as those terms that are not logarithmically enhanced at high energies but neglect all contributions of $\mathcal{O}(M_W^2/\hat{s})$. The accuracy of this approximation is discussed in detail.

After convolution with parton distribution functions, radiatively corrected predictions for transverse momentum distributions of Z bosons at hadron colliders are obtained. Concerning perturbative QCD, these predictions are based on the lowest order and thus proportional to α_{S}. To obtain realistic cross sections, higher-order QCD corrections would have to be included, in next-to-leading or even next-to-next-to-leading order.

The paper is organized as follows: In Sect. 2 the Born approximation, our conventions, the kinematics, and the parton distributions are introduced. Sect. 3 is concerned with a detailed description of the radiative corrections. In Sect. 3.1 the strategy of our calculation is described and the relevant Feynman diagrams are introduced. Sect. 3.2 is concerned with the algebraic reduction of the amplitudes to a set of basic Lorentz and Dirac structures that are multiplied by scalar form factors and scalar one-loop integrals. Subsequently the renormalization is performed (Sect. 3.3) and a compact form for the results is given (Sect. 3.4), with a decomposition into Abelian and non-Abelian contributions. Special attention is paid to the behaviour in the high-energy limit (Sect. 3.5), which can be cast into a compact form. Indeed the quadratic and linear logarithms confirm the evaluation of the Sudakov logarithms obtained earlier in Ref. [14]. Sect. 4 then contains a detailed discussion of numerical results, both for pp and $p\bar{p}$ collisions at 14 TeV and 2 TeV, respectively. The leading and next-to-leading two-loop logarithmic terms are included in this numerical analysis. We also discuss the sensitivity of the results towards the choice of the renormalization scheme and justify the use of the $\overline{\mathrm{MS}}$ scheme adopted in this paper. Sect. 5 concludes with a brief summary.

2 Conventions and kinematics

The $p_{\rm T}$ distribution of Z bosons in the reaction $h_1h_2 \to Z + \text{jet}$ is given by

$$\frac{\mathrm{d}\sigma^{h_1h_2}}{\mathrm{d}p_{\rm T}} = \sum_{i,j} \int_0^1 \mathrm{d}x_1 \int_0^1 \mathrm{d}x_2\, \theta(x_1x_2 - \hat{\tau}_{\rm min}) f_{h_1,i}(x_1,\mu^2) f_{h_2,j}(x_2,\mu^2) \frac{\mathrm{d}\hat{\sigma}^{ij}}{\mathrm{d}p_{\rm T}}, \qquad (1)$$

where $\hat{\tau}_{\rm min} = (p_{\rm T} + m_{\rm T})^2/s$, $m_{\rm T} = \sqrt{p_{\rm T}^2 + M_Z^2}$ and $\sqrt{s}$ is the collider energy. The indices i, j denote initial state partons $(q, \bar{q}, g)$ and $f_{h_1,i}(x,\mu^2)$, $f_{h_2,j}(x,\mu^2)$ are the corresponding parton distribution functions. $\hat{\sigma}^{ij}$ is the partonic cross section for the subprocess $ij \to Zk$ and the sum runs over all i, j combinations corresponding to the subprocesses

$$\bar{q}q \to Zg, \quad q\bar{q} \to Zg, \quad gq \to Zq, \quad qg \to Zq, \quad \bar{q}g \to Z\bar{q}, \quad g\bar{q} \to Z\bar{q}. \qquad (2)$$

The Mandelstam variables for the subprocess $ij \to Zk$ are defined in the standard way

$$\hat{s} = (p_i + p_j)^2, \qquad \hat{t} = (p_i - p_Z)^2, \qquad \hat{u} = (p_j - p_Z)^2. \qquad (3)$$

The momenta p_i, p_j, p_k of the partons are assumed to be massless, whereas $p_Z^2 = M_Z^2$. In terms of $x_1, x_2, p_{\rm T}$ and the collider energy $\sqrt{s}$ we have

$$\hat{s} = x_1x_2s, \qquad \hat{t} = \frac{M_Z^2 - \hat{s}}{2}(1 - \cos\theta), \qquad \hat{u} = \frac{M_Z^2 - \hat{s}}{2}(1 + \cos\theta), \qquad (4)$$

with $\cos\theta = \sqrt{1 - 4p_{\rm T}^2\hat{s}/(\hat{s} - M_Z^2)^2}$ corresponding to the cosine of the angle between the momenta p_i and p_Z in the partonic center-of-mass frame.

The angular and the $p_{\rm T}$ distribution for the unpolarized partonic subprocess $ij \to Zk$ read

$$\frac{\mathrm{d}\hat{\sigma}^{ij}}{\mathrm{d}\cos\theta} = \frac{\hat{s} - M_Z^2}{32\pi N_{ij}\hat{s}^2} \overline{\sum} |\mathcal{M}^{ij}|^2 \qquad (5)$$

and

$$\frac{\mathrm{d}\hat{\sigma}^{ij}}{\mathrm{d}p_{\rm T}} = \frac{p_{\rm T}}{8\pi N_{ij}\hat{s}|\hat{t} - \hat{u}|} \left[\overline{\sum} |\mathcal{M}^{ij}|^2 + (\hat{t} \leftrightarrow \hat{u})\right], \qquad (6)$$

where

$$\overline{\sum} = \frac{1}{4} \sum_{\rm pol} \sum_{\rm col} \qquad (7)$$

involves the sum over polarization and color as well as the average factor $1/4$ for initial-state polarization. The factor $1/N_{ij}$ in (5)-(6), with $N_{\bar{q}q} = N_{q\bar{q}} = N_{\rm c}^2$, $N_{gq} =$

$N_{qg} = N_{\bar{q}g} = N_{g\bar{q}} = N_{\rm c}(N_{\rm c}^2-1)$, and $N_{\rm c} = 3$, accounts for the initial-state colour average. The factor

$$\hat{t} - \hat{u} = (\hat{s} - M_Z^2)\cos\theta = s\sqrt{(x_1x_2 - \hat{\tau}_{\rm min})(x_1x_2 - \hat{\tau}_{\rm min} + 4p_{\rm T}m_{\rm T}/s)} \tag{8}$$

in the denominator of (6) gives rise to the so-called Jacobian peak, which arises at $\cos\theta = 0$ or, equivalently, at $x_1x_2 = \hat{\tau}_{\rm min}$ and is smeared by the integration over the parton distribution functions.

The unpolarized squared matrix elements for the processes (2) are related by the crossing-symmetry relations

$$\overline{\sum}|\mathcal{M}^{gq}|^2 = -\,\overline{\sum}|\mathcal{M}^{\bar{q}q}|^2\Big|_{\hat{s}\leftrightarrow\hat{t}}, \qquad \overline{\sum}|\mathcal{M}^{\bar{q}g}|^2 = -\,\overline{\sum}|\mathcal{M}^{\bar{q}q}|^2\Big|_{\hat{s}\leftrightarrow\hat{u}}, \tag{9}$$

and

$$\overline{\sum}|\mathcal{M}^{ji}|^2 = \overline{\sum}|\mathcal{M}^{ij}|^2\Big|_{\hat{t}\leftrightarrow\hat{u}}. \tag{10}$$

Moreover, as a result of CP symmetry,

$$\overline{\sum}|\mathcal{M}^{\bar{q}q}|^2 = \overline{\sum}|\mathcal{M}^{\bar{q}q}|^2\Big|_{\hat{t}\leftrightarrow\hat{u}}. \tag{11}$$

Using these symmetries we can write

$$\begin{aligned}\frac{{\rm d}\sigma^{h_1h_2}}{{\rm d}p_{\rm T}} = &\sum_{q=u,d,c,s,b}\int_0^1{\rm d}x_1\int_0^1{\rm d}x_2\;\theta(x_1x_2-\hat{\tau}_{\rm min})\\ &\times\Bigg\{\Big[f_{h_1,q}(x_1,\mu^2)f_{h_2,\bar{q}}(x_2,\mu^2)+(1\leftrightarrow2)\Big]\frac{{\rm d}\hat{\sigma}^{\bar{q}q}}{{\rm d}p_{\rm T}}\\ &+\Big[\Big(f_{h_1,q}(x_1,\mu^2)f_{h_2,g}(x_2,\mu^2)+f_{h_1,\bar{q}}(x_1,\mu^2)f_{h_2,g}(x_2,\mu^2)\Big)+(1\leftrightarrow2)\Big]\frac{{\rm d}\hat{\sigma}^{qg}}{{\rm d}p_{\rm T}}\Bigg\}.\end{aligned} \tag{12}$$

By means of (9) and (10) $\overline{\sum}|\mathcal{M}^{qg}|^2$ is expressed in terms of $\overline{\sum}|\mathcal{M}^{\bar{q}q}|^2$, i.e. the explicit computation of the unpolarized squared matrix element needs to be performed only for one of the six processes in (2).

To lowest order in α and $\alpha_{\rm S}$, for the $\bar{q}q \to Zg$ process [14]

$$\overline{\sum}|\mathcal{M}_0^{\bar{q}q}|^2 = 8\pi^2\alpha\alpha_{\rm S}(N_{\rm c}^2-1)\sum_{\lambda={\rm L,R}}\left(I_{q_\lambda}^Z\right)^2\frac{\hat{t}^2+\hat{u}^2+2M_Z^2\hat{s}}{\hat{t}\hat{u}}, \tag{13}$$

where $\alpha = e^2/(4\pi)$ and $\alpha_{\rm S} = g_{\rm S}^2/(4\pi)$ are the electromagnetic and the strong coupling constants and $I_{q_\lambda}^Z$ represents the eigenvalue of the generator associated with the Z boson in the representation corresponding to right-handed ($\lambda = {\rm R}$) or left-handed ($\lambda = {\rm L}$) quarks q_λ. In terms of the weak isospin $T_{q_\lambda}^3$ and the weak hypercharge Y_{q_λ}

$$I_{q_\lambda}^Z = \frac{c_{\rm W}}{s_{\rm W}}T_{q_\lambda}^3 - \frac{s_{\rm W}}{c_{\rm W}}\frac{Y_{q_\lambda}}{2}, \tag{14}$$

with the shorthands $c_\mathrm{w} = \cos\theta_\mathrm{W}$ and $s_\mathrm{w} = \sin\theta_\mathrm{W}$ for the weak mixing angle θ_W.

In general, for gauge couplings we adopt the conventions of Ref. [10]. With this notation the $gq\bar{q}$ vertex and the $Vq\bar{q}$ vertices with $V = A, Z, W^\pm$ read

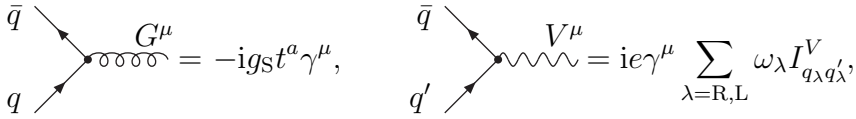

(15)

where ω_λ are the chiral projectors

$$\omega_\mathrm{R} = \frac{1}{2}(1+\gamma_5), \qquad \omega_\mathrm{L} = \frac{1}{2}(1-\gamma_5), \tag{16}$$

t^a are the Gell-Mann matrices and I^V are matrices in the weak isospin space. For diagonal matrices such as I^Z we write $I^Z_{q_\lambda q'_\lambda} = \delta_{qq'} I^Z_{q_\lambda}$. The triple gauge-bosons vertices read

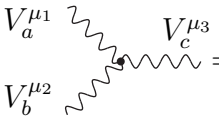

$$= \frac{e}{s_\mathrm{W}} \varepsilon^{V_a V_b V_c} [g^{\mu_1\mu_2}(k_1-k_2)^{\mu_3} + g^{\mu_2\mu_3}(k_2-k_3)^{\mu_1} + g^{\mu_3\mu_1}(k_3-k_1)^{\mu_2}]. \tag{17}$$

The definition of the antisymmetric tensor ε as well as useful group-theoretical identities can be found in App. B of Ref. [10].

3 $\mathcal{O}(\alpha)$ corrections

In this section we present the one-loop weak corrections to the process $\bar{q}q \to Zg$. The algebraic reduction to standard matrix elements and scalar integrals is described in Sect. 3.2. Renormalization, in the $\overline{\mathrm{MS}}$ and the on-shell scheme, is discussed in Sect. 3.3. In Sect. 3.4 we present analytical results for the unpolarized squared matrix elements, and the high-energy behaviour of the corrections is derived in Sect. 3.5.

3.1 Preliminaries

As discussed in the previous section, the 6 different processes relevant for $Z+1$ jet production are related by crossing symmetries. It is thus sufficient to consider only one of these processes. In the following we derive the one-loop corrections for the $\bar{q}q \to Zg$ process. The matrix element

$$\mathcal{M}_1^{\bar{q}q} = \mathcal{M}_0^{\bar{q}q} + \delta\mathcal{M}_1^{\bar{q}q} \tag{18}$$

is expressed as a function of the Mandelstam invariants

$$\hat{s} = (p_{\bar{q}} + p_q)^2, \qquad \hat{t} = (p_{\bar{q}} - p_Z)^2, \qquad \hat{u} = (p_q - p_Z)^2. \tag{19}$$

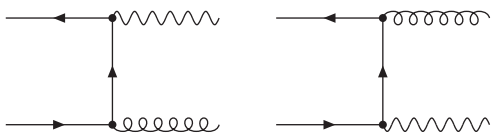

Figure 1: Tree-level Feynman diagrams for the process $\bar{q}q \to Zg$.

The Born contribution, $\mathcal{M}_0^{\bar{q}q}$, results from the t- and u-channel diagrams of Fig. 1. The loop and counterterm (CT) diagrams contributing to the corrections,

$$\delta\mathcal{M}_1^{\bar{q}q} = \delta\mathcal{M}_{1,\text{loops}}^{\bar{q}q} + \delta\mathcal{M}_{1,\text{CT}}^{\bar{q}q}, \tag{20}$$

are depicted in Fig. 2 and Fig. 3, respectively.

We do not include electromagnetic corrections, i.e. we restrict ourselves to the virtual weak contributions of $\mathcal{O}(\alpha^2\alpha_\text{S})$. In the kinematical region where the Z-boson transverse momentum is non-vanishing the emission of the gluon does not give rise to soft or collinear singularities and the (renormalized) virtual weak corrections are finite. All (real and virtual) quarks appearing in the diagrams of Fig. 2 are treated as massless[1] and diagrams involving couplings of quarks to Higgs bosons or would-be-Goldstone bosons are not considered. Quark-mixing effects are also neglected. The only quark-mass effects that we take into account are the m_t-and m_b-terms in the gauge-boson self-energies, which contribute to the counterterms.

Our calculation has been performed at the level of matrix elements and provides full control over polarization effects. However, at this level, the analytical expressions are too large to be published. Explicit results will thus be presented only for the unpolarized squared matrix elements

$$\overline{\sum}|\mathcal{M}_1^{\bar{q}q}|^2 = \overline{\sum}|\mathcal{M}_0^{\bar{q}q}|^2 + 2\text{Re}\left[\overline{\sum}\left(\mathcal{M}_0^{\bar{q}q}\right)^* \delta\mathcal{M}_1^{\bar{q}q}\right] + \mathcal{O}(\alpha^3\alpha_\text{S}). \tag{21}$$

3.2 Algebraic reduction

The matrix element (18) has the general form

$$\mathcal{M}_1^{\bar{q}q} = \mathrm{i}\, e\, g_\text{S}\, t^a \sum_{\lambda=\text{R,L}} \bar{v}(p_{\bar{q}})\mathcal{M}_1^{\lambda,\mu\nu}\omega_\lambda u(p_q)\, \varepsilon_\mu^*(p_Z)\varepsilon_\nu^*(p_g), \tag{22}$$

where the γ^5-terms are isolated in the chiral projectors ω_λ defined in (16). Since

[1] Quark-mass contributions are of $\mathcal{O}(m_q^2/M_Z^2)$ and can thus be neglected for $q \neq t$. The contributions of $\mathcal{O}(m_t^2/M_Z^2)$ arising from those diagrams of Fig. 2 that involve initial-state b quarks and virtual W bosons are large at the partonic level. However, at the hadronic level, also these contributions can be neglected since the subprocesses initiated by b quarks are suppressed by the very small b-quark density of protons.

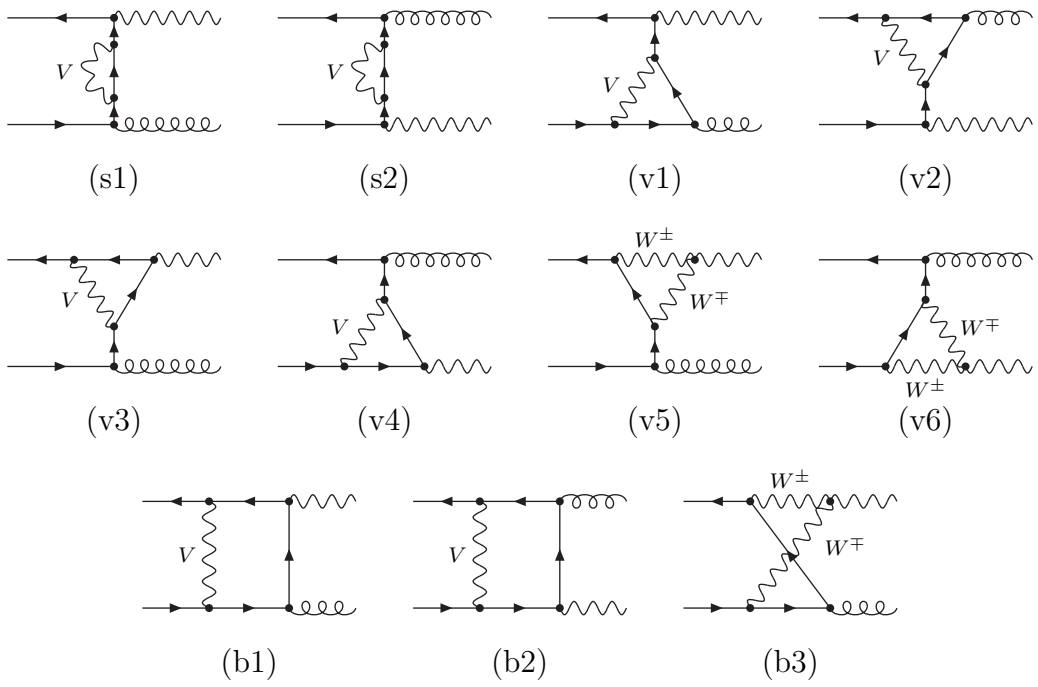

Figure 2: One-loop Feynman diagrams for the process $\bar{q}q \to Zg$. The diagrams v5, v6 and b3 involve only charged weak bosons, $W^{\pm}$, whereas the other diagrams receive contributions from neutral and charged weak bosons, $V = Z, W^{\pm}$.

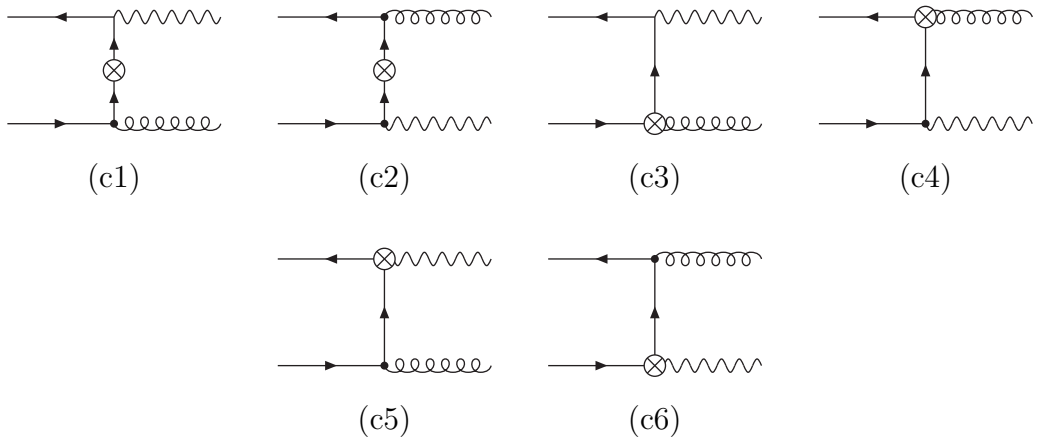

Figure 3: Counterterm diagrams for the process $\bar{q}q \to Zg$.

we treat quarks as massless, $\mathcal{M}_1^{\lambda,\mu\nu}$ consists of terms involving an odd number of matrices γ^ρ with $\rho = 0,\ldots,3$. The polarization dependence of the quark spinors and gauge-boson polarization vectors is implicitly understood.

In analogy to (18), (20) we write

$$\mathcal{M}_1^{\lambda,\mu\nu} = \mathcal{M}_0^{\lambda,\mu\nu} + \delta\mathcal{M}_1^{\lambda,\mu\nu}, \qquad \delta\mathcal{M}_1^{\lambda,\mu\nu} = \delta\mathcal{M}_{1,\text{loops}}^{\lambda,\mu\nu} + \delta\mathcal{M}_{1,\text{CT}}^{\lambda,\mu\nu}. \tag{23}$$

The unpolarized squared matrix element (21) is obtained from $\mathcal{M}_0^{\lambda,\mu\nu}$ and $\delta\mathcal{M}_1^{\lambda,\mu\nu}$ using

$$\begin{aligned}\overline{\sum}\left(\mathcal{M}_0^{\bar{q}q}\right)^* \delta\mathcal{M}_1^{\bar{q}q} = \pi^2\alpha\alpha_\text{S}(N_c^2-1)\sum_{\lambda=\text{R,L}} \text{Tr}\left[\not{p}_q \overline{\mathcal{M}}_0^{\lambda,\mu\nu} \not{p}_{\bar{q}} \delta\mathcal{M}_1^{\lambda,\mu'\nu'}\right] \\ \times g_{\nu\nu'}\left(g_{\mu\mu'} - \frac{p_{Z\mu}p_{Z\mu'}}{M_Z^2}\right).\end{aligned} \tag{24}$$

The Born contribution reads

$$\mathcal{M}_0^{\lambda,\mu\nu} = I_{q_\lambda}^Z \mathcal{S}_0^{\mu\nu}, \qquad \mathcal{S}_0^{\mu\nu} = \frac{\gamma^\mu(\not{p}_Z - \not{p}_{\bar{q}})\gamma^\nu}{\hat{t}} + \frac{\gamma^\nu(\not{p}_g - \not{p}_{\bar{q}})\gamma^\mu}{\hat{u}}, \tag{25}$$

and is simply proportional to the gauge group generator I^Z, which determines the dependence of $\mathcal{M}_0$ on the weak mixing angle, the chirality ($\lambda = \text{R,L}$) and the weak isospin of quarks (u,d). Let us now consider the combinations of gauge group generators that appear in the loop diagrams of Fig. 2. The diagrams involving virtual Z bosons are simply proportional to $(I^Z)^3$. Instead, the diagrams with virtual W bosons (diagrams s1–b3 with $V = W^\pm$) yield combinations of non-commuting gauge-group generators $I^Z, I^{W^\pm}$ and triple gauge-boson couplings $\varepsilon^{W^\pm W^\mp Z}$, which can be expressed as[2]

$$I^Z I^{W^\pm} I^{W^\mp} = I^{W^\pm} I^{W^\mp} I^Z \qquad \text{(diagrams s1, s2, v1, v2)}, \tag{26}$$

$$\frac{\text{i}}{s_\text{W}} \varepsilon^{W^\pm W^\mp Z} I^{W^\pm} I^{W^\mp} = \frac{c_\text{W}}{s_\text{W}^3} T^3 \qquad \text{(diagrams v5, v6, b3)}, \tag{27}$$

$$I^{W^\pm} I^Z I^{W^\mp} = I^Z I^{W^\pm} I^{W^\mp} - \frac{c_\text{W}}{s_\text{W}^3} T^3 \qquad \text{(diagrams v3, v4, b1, b2)}, \tag{28}$$

where fermionic indices of the generators I^V as well as summations over $W^\pm$ are implicitly understood. The contribution of the loop diagrams of Fig. 2 can thus be expressed as a linear combination of I^Z and T^3,

$$\delta\mathcal{M}_{1,\text{loops}}^{\lambda,\mu\nu} = \frac{\alpha}{4\pi}\left[I_{q_\lambda}^Z \sum_{V=\text{Z,W}^\pm} \left(I^V I^{\bar{V}}\right)_{q_\lambda} \delta\mathcal{A}_{1,\text{A}}^{\mu\nu}(M_V^2) + \frac{c_\text{W}}{s_\text{W}^3} T_{q_\lambda}^3 \, \delta\mathcal{A}_{1,\text{N}}^{\mu\nu}(M_W^2)\right], \tag{29}$$

[2]The relation (27) can be derived from Eqs. (B.5) and (B.24) in Ref. [10] whereas (28) follows from (27) combined with the commutation relation $[I^{W^\pm}, I^Z] = -(\text{i}/s_\text{W})\varepsilon^{W^\pm W^\mp Z} I^{W^\pm}$.

with

$$\left(I^Z I^Z\right)_{q_\lambda} = \left(I^Z_{q_\lambda}\right)^2, \qquad \sum_{V=W^\pm} \left(I^V I^{\bar{V}}\right)_{q_\lambda} \equiv \left(I^{W^\pm} I^{W^\mp}\right)_{q_\lambda} = \frac{\delta_{\lambda \mathrm{L}}}{2 s_\mathrm{W}^2}. \tag{30}$$

The amplitudes $\delta\mathcal{A}^{\mu\nu}_{1,\mathrm{A/N}}(M_V^2)$ are denoted as the Abelian (A) and non-Abelian (N) contributions, since the latter originates from the non-commutativity of weak interactions, whereas the former is present also in Abelian theories.

These amplitudes have been reduced algebraically using the Dirac equation, the identity $p^\mu \varepsilon_\mu(p) = 0$ for gauge-boson polarization vectors and Dirac algebra. Moreover, tensor loop integrals have been reduced to scalar ones by means of the Passarino-Veltman technique. The result has been expressed in the form

$$\delta\mathcal{A}^{\mu\nu}_{1,\mathrm{A/N}}(M_V^2) = \sum_{i=1}^{10} \sum_{j=0}^{14} \mathcal{F}^{ij}_{\mathrm{A/N}}(M_V^2) \mathcal{S}_i^{\mu\nu} J_j(M_V^2), \tag{31}$$

where the form factors $\mathcal{F}^{ij}_{\mathrm{A/N}}(M_V^2)$ are rational functions of Mandelstam invariants and masses. The tensors

$$\begin{aligned}
\mathcal{S}_1^{\mu\nu} &= \gamma^\mu (\not{p}_Z - \not{p}_{\bar{q}}) \gamma^\nu, \\
\mathcal{S}_2^{\mu\nu} &= (\not{p}_Z - \not{p}_g) g^{\mu\nu}, \\
\mathcal{S}_3^{\mu\nu} &= \gamma^\mu p_Z^\nu, \\
\mathcal{S}_4^{\mu\nu} &= -\gamma^\nu p_g^\mu, \\
\mathcal{S}_5^{\mu\nu} &= \gamma^\mu p_q^\nu, \\
\mathcal{S}_6^{\mu\nu} &= -\gamma^\nu p_{\bar{q}}^\mu, \\
\mathcal{S}_7^{\mu\nu} &= (\not{p}_Z - \not{p}_g) p_g^\mu p_Z^\nu, \\
\mathcal{S}_8^{\mu\nu} &= (\not{p}_Z - \not{p}_g) p_{\bar{q}}^\mu p_q^\nu, \\
\mathcal{S}_9^{\mu\nu} &= (\not{p}_Z - \not{p}_g) p_g^\mu p_q^\nu, \\
\mathcal{S}_{10}^{\mu\nu} &= (\not{p}_Z - \not{p}_g) p_{\bar{q}}^\mu p_Z^\nu,
\end{aligned} \tag{32}$$

correspond to the massless subset of the standard matrix elements of Ref. [16] and, apart from $J_0(M_V^2) = 1$, the functions $J_j(M_V^2)$ represent the scalar one-loop integrals resulting from the reduction.[3] The one- and two-point functions,

$$\begin{aligned}
J_1(M_V^2) &= A_0(M_V^2), \\
J_2(M_V^2) &= B_0(M_Z^2; 0, 0), \\
J_3(M_V^2) &= B_0(M_Z^2; M_V^2, M_V^2), \\
J_4(M_V^2) &= B_0(\hat{s}; 0, 0), \\
J_5(M_V^2) &= B_0(\hat{u}; M_V^2, 0), \\
J_6(M_V^2) &= B_0(\hat{t}; M_V^2, 0),
\end{aligned} \tag{33}$$

[3]For the scalar integrals A_0, B_0, C_0 and D_0 we adopt the notation of `FeynCalc` [17]. However, we choose their normalization according to Ref. [16], i.e. we include the factor $(2\pi\mu)^{4-D}$ which is omitted in the conventions of `FeynCalc`.

are ultraviolet (UV) divergent. The resulting poles, in $D = 4 - 2\varepsilon$ dimensions, amount to

$$\delta\mathcal{A}^{\mu\nu}_{1,\mathrm{A}}(M_V^2)\Big|_{\mathrm{UV}} = \frac{1}{\varepsilon}\mathcal{S}_0^{\mu\nu}, \qquad \delta\mathcal{A}^{\mu\nu}_{1,\mathrm{N}}(M_V^2)\Big|_{\mathrm{UV}} = \frac{2}{\varepsilon}\mathcal{S}_0^{\mu\nu}, \tag{34}$$

where $\mathcal{S}_0^{\mu\nu}$ is the Born amplitude defined in (25). These singularities are cancelled by the counterterms (see Sect. 3.3). The remaining loop integrals are free from UV singularities. The three-point functions

$$\begin{aligned}
J_7(M_V^2) &= C_0(\hat{s}, 0, 0; 0, 0, M_V^2),\\
J_8(M_V^2) &= C_0(\hat{u}, M_Z^2, 0; M_V^2, 0, 0),\\
J_9(M_V^2) &= C_0(\hat{u}, M_Z^2, 0; 0, M_V^2, M_V^2),\\
J_{10}(M_V^2) &= C_0(\hat{t}, M_Z^2, 0; M_V^2, 0, 0),\\
J_{11}(M_V^2) &= C_0(\hat{t}, M_Z^2, 0; 0, M_V^2, M_V^2)
\end{aligned} \tag{35}$$

are finite for non-vanishing Z-boson transverse momentum. In addition, we obtain the three- and four-point functions

$$\begin{aligned}
&C_0(\hat{u}, 0, 0; M_V^2, 0, 0), \qquad D_0(0, 0, M_Z^2, 0, \hat{u}, \hat{s}; M_V^2, 0, 0, 0),\\
&C_0(\hat{t}, 0, 0; M_V^2, 0, 0), \qquad D_0(0, 0, M_Z^2, 0, \hat{t}, \hat{s}; M_V^2, 0, 0, 0),\\
&C_0(\hat{s}, M_Z^2, 0; 0, 0, 0), \qquad D_0(M_Z^2, 0, 0, 0, \hat{t}, \hat{u}; M_V^2, M_V^2, 0, 0),
\end{aligned} \tag{36}$$

which result from the reduction of the box diagrams b1–b3. As a consequence of vanishing quark masses, these latter integrals (36) give rise to mass singularities of collinear nature. Such singularities originate from the propagators of those massless (virtual) quarks that couple to the massless (real) gluon,

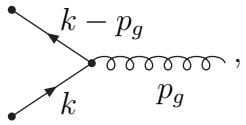

, (37)

specifically from the integration region with $k^\mu \to x p_g^\mu$, where the momenta of these quarks become collinear to the gluon momentum. However, the box diagrams are finite since the quark-gluon vertex (37) yields

$$(\not{k} - \not{p}_g)\not{\varepsilon}_g \not{k} \to x(x-1)\not{p}_g \not{\varepsilon}_g \not{p}_g = x(x-1)\left[2\not{p}_g (p_g.\varepsilon_g) - \not{\varepsilon}_g p_g^2\right] = 0, \tag{38}$$

in the collinear limit. Indeed, as a consequence of cancellations between the singularities from the C_0 and the D_0 functions in (36), our result is finite.

In order to control these cancellations at the analytical and numerical level, we have regulated the singularities by means of an infinitesimal quark-mass parameter λ. Then, using Ref. [18] we have expressed the singular parts of D_0 functions through singular C_0 functions and checked that these cancel against the singular C_0 functions

resulting from the reduction. Finally we have written our result in terms of finite combinations of D_0 and C_0 functions,

$$
\begin{aligned}
J_{12}(M_V^2) &= D_0(0,0,M_Z^2,0,\hat{u},\hat{s};M_V^2,0,\lambda^2,0) - \frac{(\hat{u}-M_Z^2)C_0(\hat{u},M_Z^2,0;M_V^2,\lambda^2,0)}{\hat{s}\hat{u}+(\hat{t}+\hat{u})M_V^2} \\
&\quad - \frac{\hat{u}C_0(\hat{u},0,0;M_V^2,\lambda^2,0)+(\hat{s}-M_Z^2)C_0(\hat{s},M_Z^2,0;0,0,\lambda^2)}{\hat{s}\hat{u}+(\hat{t}+\hat{u})M_V^2}, \\
J_{13}(M_V^2) &= D_0(0,0,M_Z^2,0,\hat{t},\hat{s};M_V^2,0,\lambda^2,0) - \frac{(\hat{t}-M_Z^2)C_0(\hat{t},M_Z^2,0;M_V^2,\lambda^2,0)}{\hat{s}\hat{t}+(\hat{t}+\hat{u})M_V^2} \\
&\quad - \frac{\hat{t}C_0(\hat{t},0,0;M_V^2,\lambda^2,0)+(\hat{s}-M_Z^2)C_0(\hat{s},M_Z^2,0;0,0,\lambda^2)}{\hat{s}\hat{t}+(\hat{t}+\hat{u})M_V^2}, \\
J_{14}(M_V^2) &= D_0(M_Z^2,0,0,0,\hat{t},\hat{u};M_V^2,M_V^2,0,\lambda^2) \\
&\quad - \frac{\hat{t}C_0(\hat{t},0,0;M_V^2,0,\lambda^2)+\hat{u}C_0(\hat{u},0,0;M_V^2,\lambda^2,0)}{\hat{t}\hat{u}-(\hat{t}+\hat{u})M_V^2},
\end{aligned}
\tag{39}
$$

which correspond to the finite parts of four-point integrals expressed as $D_0 - D_0^{\mathrm{sing}}$, with the singular parts D_0^{sing} in terms of C_0 functions. It was checked that the functions J_{12}, J_{13}, J_{14} are indeed finite and numerically stable for $\lambda/M_Z \ll 1$. The numerical results presented in Sect. 4 have been obtained using $\lambda/M_Z = 10^{-6}$.

3.3 Renormalization

The renormalization of the process $\bar{q}q \to Zg$ is provided by the diagrams depicted in Fig. 3. The counterterms (CTs) that are responsible for the contributions of diagrams c1, c2, c3 and c4 read

$$= \mathrm{i}\not{p} \sum_{\lambda=\mathrm{R,L}} \omega_\lambda \delta Z_{q_\lambda},$$

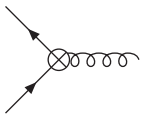

$$= -\mathrm{i}g_\mathrm{S} t^a \gamma^\mu \sum_{\lambda=\mathrm{R,L}} \omega_\lambda \delta Z_{q_\lambda}. \tag{40}$$

Since there is no $\mathcal{O}(\alpha)$-contribution to the renormalization of the strong coupling constant g_S, these CTs depend only on the fermionic wave-function renormalization constants δZ_{q_λ} [see (43)]. Their combined contribution to the $\bar{q}q \to Zg$ process, i.e. the sum of diagrams c1, c2, c3 and c4, vanishes. The renormalization of the $\bar{q}q \to Zg$ process is thus provided by the diagrams c5, c6, which originate from the $Zq\bar{q}$ counterterm,

$$= \mathrm{i}e\gamma^\mu \sum_{\lambda=\mathrm{R,L}} \omega_\lambda \left[I_{q_\lambda}^Z \left(\delta Z_{q_\lambda} + \delta C_{q_\lambda}^\mathrm{A} \right) + \frac{c_\mathrm{W}}{s_\mathrm{W}} T_{q_\lambda}^3 \, \delta C_{q_\lambda}^\mathrm{N} \right], \tag{41}$$

and yield

$$\delta \mathcal{M}_{1,\mathrm{CT}}^{\lambda,\mu\nu} = \left[I_{q_\lambda}^Z \left(\delta Z_{q_\lambda} + \delta C_{q_\lambda}^\mathrm{A} \right) + \frac{c_\mathrm{W}}{s_\mathrm{W}} T_{q_\lambda}^3 \, \delta C_{q_\lambda}^\mathrm{N} \right] \mathcal{S}_0^{\mu\nu}, \tag{42}$$

with $\mathcal{S}_0^{\mu\nu}$ defined as in (25). As indicated in (41), the $Zq\bar{q}$ CT can be expressed as a linear combination of $I^Z_{q_\lambda}$ and $T^3_{q_\lambda}$, analogous to (29). The corresponding coefficients involve the wave-function renormalization constants of massless chiral quarks,[4]

$$\delta Z_{q_\lambda} = -\mathrm{Re}\left[\Sigma^{q,\lambda}(0)\right] = \frac{\alpha}{4\pi}\sum_{V=\mathrm{Z},\mathrm{W}^\pm}\left(I^V I^{\bar{V}}\right)_{q_\lambda}\left[\frac{3}{2} - \frac{A_0(M_V^2)}{M_V^2}\right], \tag{43}$$

where only weak corrections ($V = \mathrm{Z}, \mathrm{W}^\pm$) are included, and the following combinations of renormalization constants

$$\begin{aligned}
\delta C^{\mathrm{A}}_{q_\lambda} &= \frac{1}{2}\left(\delta Z_{ZZ} + \frac{c_\mathrm{W}}{s_\mathrm{W}}\delta Z_{AZ} + \frac{\delta e^2}{e^2} - \frac{1}{s_\mathrm{W}^2}\frac{\delta c_\mathrm{W}^2}{c_\mathrm{W}^2}\right), \\
\delta C^{\mathrm{N}}_{q_\lambda} &= -\frac{1}{2 s_\mathrm{W} c_\mathrm{W}}\delta Z_{AZ} + \frac{1}{s_\mathrm{W}^2}\frac{\delta c_\mathrm{W}^2}{c_\mathrm{W}^2}.
\end{aligned} \tag{44}$$

The renormalization constants associated with the Z-boson wave function read

$$\delta Z_{ZZ} = -\mathrm{Re}\left.\frac{\partial \Sigma_\mathrm{T}^{ZZ}(p^2)}{\partial p^2}\right|_{p^2=M_Z^2}, \qquad \delta Z_{AZ} = -2\mathrm{Re}\left[\frac{\Sigma_\mathrm{T}^{\mathrm{AZ}}(M_Z^2)}{M_Z^2}\right] \tag{45}$$

and have been evaluated using the self-energies of Ref. [16].

For the renormalization of e and c_W we have considered two different schemes, the $\overline{\mathrm{MS}}$ and the on-shell scheme. In the $\overline{\mathrm{MS}}$ scheme, the CTs for e and c_W read

$$\begin{aligned}
\frac{\delta c_\mathrm{W}^2}{c_\mathrm{W}^2} &\overset{\overline{\mathrm{MS}}}{=} -\frac{\alpha}{4\pi}\bar{\Delta}_\mathrm{UV}\left[\frac{19 + 22 s_\mathrm{W}^2}{6 c_\mathrm{W}^2} + 2(\rho - 1)\right], \\
\frac{\delta e^2}{e^2} &\overset{\overline{\mathrm{MS}}}{=} \frac{\alpha}{4\pi}\bar{\Delta}_\mathrm{UV}\left[\frac{11}{3} + \left(\frac{2}{s_\mathrm{W}^2} - 4\right)(\rho - 1)\right],
\end{aligned} \tag{46}$$

where

$$\bar{\Delta}_\mathrm{UV} = 1/\varepsilon - \gamma_\mathrm{E} + \log(4\pi) + \log\left(\frac{\mu_\mathrm{R}^2}{M_Z^2}\right) \tag{47}$$

in $D = 4 - 2\varepsilon$ dimensions and $\rho = M_W^2/(c_\mathrm{W}^2 M_Z^2)$. In (47) we have included a logarithmic term that renders the renormalized amplitude independent of the scale μ_R of dimensional regularization. This is equivalent to the choice $\mu_\mathrm{R} = M_Z$ within the usual $\overline{\mathrm{MS}}$ scheme. We also note that the counterterms (46) contain contributions proportional to $(\rho - 1)$ which depend on the relation between M_W and M_Z. In principle, in an $\mathcal{O}(\alpha)$ $\overline{\mathrm{MS}}$ calculation the value of the W mass, which appears

[4] $\Sigma^{q,\lambda}(p^2)$ are the chiral components of the one-particle irreducible two-point function of massless fermions,

$$\Gamma^{q\bar{q}}(p) = \mathrm{i}\not{p}\left[1 + \sum_{\lambda=\mathrm{R},\mathrm{L}}\omega_\lambda \Sigma^{q,\lambda}(p^2)\right].$$

only in loop diagrams, should be derived from the on-shell Z-boson mass and the $\overline{\rm MS}$ mixing angle using the tree-level relation $M_W = c_{\rm w} M_Z$. In this case the $(\rho-1)$ contributions in (46) would vanish. However, it seems more natural to use the on-shell value of M_W as an input parameter in our calculation. This violates the tree-level mass relation and introduces loop corrections that are implicitly contained in the numerical value of M_W. Their effect on our $\mathcal{O}(\alpha)$ predictions is formally of $\mathcal{O}(\alpha^2)$ since M_W does not contribute at tree level. This procedure is thus consistent at $\mathcal{O}(\alpha)$. However, it affects also those $1/\varepsilon$ poles that appear in δZ_{AZ} since they depend on M_W. Such singularities give rise to terms proportional to $(\rho-1)/\varepsilon$ that are again, formally, of $\mathcal{O}(\alpha^2)$ and are compensated by the $(\rho-1)$ terms that we have introduced in (46). This procedure removes all higher-order effects from the divergent part of the counterterms (44), which becomes independent of $(\rho-1)$, and ensures the cancellation of the singularities (34) originating from the loop diagrams for arbitrary values of ρ.

In the on-shell (OS) scheme, the weak mixing angle is defined as $c_{\rm w}^2 = M_W^2/M_Z^2$ and the corresponding CT reads

$$\frac{\delta c_{\rm w}^2}{c_{\rm w}^2} \stackrel{\rm OS}{=} \mathrm{Re}\left[\frac{\Sigma_{\rm T}^{WW}(M_W^2)}{M_W^2} - \frac{\Sigma_{\rm T}^{ZZ}(M_Z^2)}{M_Z^2}\right]. \tag{48}$$

As on-shell input parameter for the electromagnetic coupling constant we used $\alpha = \alpha(M_Z^2)$, defined as

$$\alpha(M_Z^2) = \frac{\alpha(0)}{1-\Delta\alpha(M_Z^2)}, \qquad \Delta\alpha(M_Z^2) = \mathrm{Re}\left[\Pi_{\rm ferm}^{AA}(0) - \Pi_{\rm ferm}^{AA}(M_Z^2)\right], \tag{49}$$

where $\alpha(0) = e(0)^2/(4\pi)$ is the fine-structure constant in the Thompson limit and $\Pi_{\rm ferm}^{AA}$ represents the fermionic contribution to the photonic vacuum polarization. The CT associated with $e^2 = 4\pi\alpha(M_Z^2)$ is given by

$$\frac{\delta e^2}{e^2} \stackrel{\rm OS}{=} \frac{\delta e(0)^2}{e(0)^2} - \Delta\alpha(M_Z^2) = \mathrm{Re}\left[\Pi_{\rm fer}^{AA}(M_Z^2)\right] + \Pi_{\rm bos}^{AA}(0) - \frac{2s_{\rm w}}{c_{\rm w}}\frac{\Sigma_{\rm T}^{AZ}(0)}{M_Z^2}, \tag{50}$$

where $\delta e(0)$ is the CT in the Thompson limit, and $\Pi_{\rm bos}^{AA}(0)$ represents the bosonic contribution to the photon propagator.

Independently of the renormalization scheme, the above CTs yield the ultraviolet singularities[5]

$$\delta Z_{q_\lambda}\big|_{\rm UV} = -\frac{\alpha}{4\pi}\frac{1}{\varepsilon}\sum_{V=\rm Z,W^\pm}\left(I^V I^{\bar V}\right)_{q_\lambda}, \quad \delta C_{q_\lambda}^{\rm A}\Big|_{\rm UV} = 0, \quad \delta C_{q_\lambda}^{\rm N}\Big|_{\rm UV} = -\frac{\alpha}{2\pi s_{\rm w}^2}\frac{1}{\varepsilon} \tag{51}$$

that cancel the $1/\varepsilon$ poles (34) originating from the loop diagrams. The scheme dependence of the complete result is discussed in Sect. 4.

[5]Note that $\delta C_{q_\lambda}^{\rm A}$ is free from ultraviolet singularities, i.e. the pole associated with the Abelian coupling structure in (42) results exclusively from the fermionic wave-function renormalization constant δZ_{q_λ} whereas the poles originating from the renormalization of the electroweak coupling constants $(\delta e, \delta c_{\rm w})$ and the Z-boson field renormalization constants $(\delta Z_{ZZ}, \delta Z_{AZ})$ cancel in $\delta C_{q_\lambda}^{\rm A}$.

3.4 Result

Let us present the complete $\mathcal{O}(\alpha^2\alpha_{\rm S})$ result for the unpolarized squared matrix element (21) for the $\bar{q}q \to Zg$ process. Combining the contributions (25), (29), (42), and using (24) we obtain

$$\begin{aligned}\overline{\sum}|\mathcal{M}_1|^2 &= 8\pi^2\alpha\alpha_{\rm S}(N_{\rm c}^2-1)\\ &\times \sum_{\lambda={\rm R,L}}\Bigg\{\left(I^Z_{q_\lambda}\right)^2\left[H_0\left(1+2\delta C^{\rm A}_{q_\lambda}\right)+\frac{\alpha}{2\pi}\sum_{V={\rm Z,W^\pm}}\left(I^V I^{\bar{V}}\right)_{q_\lambda} H_1^{\rm A}(M_V^2)\right]\\ &+\frac{c_{\rm W}}{s_{\rm W}}T^3_{q_\lambda} I^Z_{q_\lambda}\left[2H_0\delta C^{\rm N}_{q_\lambda}+\frac{\alpha}{2\pi}\frac{1}{s^2_{\rm W}}H_1^{\rm N}(M_W^2)\right]\Bigg\},\end{aligned} \tag{52}$$

where the coupling factors are specified by (14) and (30), and

$$H_0 = \frac{1}{8}{\rm Tr}\left[\not{p}_q\,\overline{\mathcal{S}}_0^{\mu\nu}\,\not{p}_{\bar{q}}\,\mathcal{S}_0^{\mu'\nu'}\right] g_{\nu\nu'}\left(g_{\mu\mu'}-\frac{p_{Z\mu}p_{Z\mu'}}{M_Z^2}\right) = \frac{\hat{t}^2+\hat{u}^2+2\hat{s}M_Z^2}{\hat{t}\hat{u}} \tag{53}$$

represents the Born contribution. The counterterms $\delta C^{\rm A/N}_{q_\lambda}$ are defined in (44)–(50). $H_1^{\rm A/N}(M_V^2)$ are the Abelian (A) and non-Abelian (N) contributions resulting from the loop diagrams of Fig. 2 and the fermionic wave-function renormalization constants (43). These functions can be written as

$$H_1^{\rm A/N}(M_V^2) = {\rm Re}\left\{\sum_{j=0}^{14}\left[K_j^{\rm A/N}(M_V^2)+K^{\rm A/N}_{{\rm WF},j}(M_V^2)\right]J_j(M_V^2)\right\}, \tag{54}$$

where $J_0(M_V^2)=1$ and the remaining $J_j(M_V^2)$ are the loop integrals defined in (33), (35), (39). The fermionic wave-function renormalization constants yield [cf. (43)]

$$K^{\rm A}_{{\rm WF},0}(M_V^2) = \frac{3}{2}H_0, \qquad K^{\rm A}_{{\rm WF},1}(M_V^2) = -\frac{1}{M_V^2}H_0, \tag{55}$$

and $K^{\rm A/N}_{{\rm WF},i}(M_V^2)=0$ otherwise. The coefficients resulting from the loop integrals of Fig. 2 read

$$K_j^{\rm A/N}(M_V^2) = \frac{1}{8}\sum_{i=1}^{10}\mathcal{F}^{ij}_{\rm A/N}(M_V^2)\,{\rm Tr}\left[\not{p}_q\,\overline{\mathcal{S}}_0^{\mu\nu}\,\not{p}_{\bar{q}}\,\mathcal{S}_i^{\mu'\nu'}\right] g_{\nu\nu'}\left(g_{\mu\mu'}-\frac{p_{Z\mu}p_{Z\mu'}}{M_Z^2}\right), \tag{56}$$

where $\mathcal{F}^{ij}_{\rm A/N}(M_V^2)$ are the form factors of (31). The explicit expressions for these coefficients are presented in Appendix A.

In fact, as a consequence of Ward identities (see Sect. 3.6), the contributions of the $p_{Z\mu}p_{Z\mu'}/M_Z^2$ terms in (53) and (56) are equal zero. We note that the contributions of right- and left-handed quarks to the unpolarized squared matrix element (52) can be easily recognized as the terms with $\lambda={\rm R}$ and $\lambda={\rm L}$, respectively.

3.5 High-energy limit

In this section we discuss the behaviour of the corrections (52) to the $\bar{q}q \to Zg$ process in the high-p_{T} region. More specifically, we derive approximate expressions for the functions $H_1^{\mathrm{A/N}}$ and the counterterms $\delta C_{q_\lambda}^{\mathrm{A/N}}$ for the case where all energy scales are much higher than the weak-boson mass scale, i.e. in the limit where $M_W^2/\hat{s} \to 0$ and $\hat{t}/\hat{s}$, $\hat{u}/\hat{s}$ are constant.

In this approximation, which is applicable for transverse momenta of order of 100 GeV and beyond, the one-loop weak corrections are strongly enhanced by logarithms of the form $\log(\hat{s}/M_W^2)$. The logarithmically enhanced part of the corrections, which constitutes the so-called next-to-leading logarithmic (NLL) approximation, was already presented in Ref. [14]. This NLL part consists of double- and single-logarithmic terms that result from the functions $H_1^{\mathrm{A/N}}$ in (52) and read[6] [14]

$$\begin{aligned} H_1^{\mathrm{N}}(M_W^2) &\overset{\mathrm{NLL}}{=} -\left[\log^2\left(\frac{|\hat{t}|}{M_W^2}\right) + \log^2\left(\frac{|\hat{u}|}{M_W^2}\right) - \log^2\left(\frac{|\hat{s}|}{M_W^2}\right)\right] H_0, \\ H_1^{\mathrm{A}}(M_V^2) &\overset{\mathrm{NLL}}{=} -\left[\log^2\left(\frac{|\hat{s}|}{M_W^2}\right) - 3\log\left(\frac{|\hat{s}|}{M_W^2}\right)\right] H_0, \end{aligned} \tag{57}$$

whereas the counterterms do not contribute to the NLL approximation, i.e.

$$\delta C_{q_\lambda}^{\mathrm{A}} \overset{\mathrm{NLL}}{=} \delta C_{q_\lambda}^{\mathrm{N}} \overset{\mathrm{NLL}}{=} 0. \tag{58}$$

The NLL corrections (57) are proportional to the Born contribution H_0 defined in (53). The above result is free from logarithms associated with the running of the electroweak coupling constants. Also no single logarithms originating from virtual collinear weak bosons that couple to the final-state Z boson appear in (57). This is a general feature of gauge-boson production processes [9, 10].

In the following, we provide the complete asymptotic behaviour of the weak corrections, which includes, in addition to double and single logarithms, also those contributions that are not logarithmically enhanced in the high-energy limit. This constitutes formally the next-to-next-to-leading logarithmic (NNLL) approximation and provides a precision of order $(M_W^2/\hat{s})\log^2(\hat{s}/M_W^2)$.

Let us first consider the functions $H_1^{\mathrm{A/N}}$ in (52), which result from the loop diagrams of Fig. 2 and the fermionic wave-function renormalization. The asymptotic behaviour of these functions was derived using the general results of Ref. [19] for the high-energy limit of one-loop integrals. In addition, in order to simplify the

[6] The correspondence between (52), (57) and (5), (10) of Ref. [14] can be easily seen by means of the relation

$$\sum_{V=\mathrm{Z,W^\pm}} \left(I^V I^{\bar{V}}\right)_{q_\lambda} = C_{q_\lambda}^{\mathrm{ew}} - Q_q^2$$

where $C_{q_\lambda}^{\mathrm{ew}}$ is the electroweak Casimir operator and the $-Q_q^2$ term represents the subtraction of the electromagnetic contributions [14]. We also recall that the result of Ref. [14] is based on the equal-mass approximation, $M_Z = M_W$.

dependence of the result on the masses of the Z and W bosons, we have performed an expansion in the Z-W mass difference using $s_{\rm w}^2 = 1 - M_W^2/M_Z^2$ as the expansion parameter and keeping only terms up to the first order in $s_{\rm w}^2$.

The resulting NNLL expressions for $H_1^{\rm N}(M_W^2)$, $H_1^{\rm A}(M_W^2)$ and $H_1^{\rm A}(M_Z^2)$ have the general form

$$H_1^{\rm A/N}(M_V^2) \stackrel{\rm NNLL}{=} {\rm Re}\left[g_0^{\rm A/N}(M_V^2)\,\frac{\hat{t}^2+\hat{u}^2}{\hat{t}\hat{u}} + g_1^{\rm A/N}(M_V^2)\,\frac{\hat{t}^2-\hat{u}^2}{\hat{t}\hat{u}} + g_2^{\rm A/N}(M_V^2)\right], \quad (59)$$

i.e. they involve the function $(\hat{t}^2+\hat{u}^2)/\hat{t}\hat{u}$, which corresponds to the high-energy limit of the Born contribution H_0 [see (53)], and two other rational functions of the Mandelstam invariants, which describe different angular dependences. The functions $g_i^{\rm A/N}$ consist of logarithms of the kinematical variables and constants. For the non-Abelian contribution $H_1^{\rm N}(M_W^2)$ we obtain

$$\begin{aligned}
g_0^{\rm N}(M_W^2) &= 2\bar{\Delta}_{\rm UV} + \log^2\left(\frac{-\hat{s}}{M_W^2}\right) - \log^2\left(\frac{-\hat{t}}{M_W^2}\right) - \log^2\left(\frac{-\hat{u}}{M_W^2}\right) + \log^2\left(\frac{\hat{t}}{\hat{u}}\right) \\
&\quad - \frac{3}{2}\left[\log^2\left(\frac{\hat{t}}{\hat{s}}\right) + \log^2\left(\frac{\hat{u}}{\hat{s}}\right)\right] - \frac{20\pi^2}{9} - \frac{2\pi}{\sqrt{3}} + 4, \\
g_1^{\rm N}(M_W^2) &= \frac{1}{2}\left[\log^2\left(\frac{\hat{u}}{\hat{s}}\right) - \log^2\left(\frac{\hat{t}}{\hat{s}}\right)\right], \\
g_2^{\rm N}(M_W^2) &= -2\left[\log^2\left(\frac{\hat{t}}{\hat{s}}\right) + \log^2\left(\frac{\hat{u}}{\hat{s}}\right) + \log\left(\frac{\hat{t}}{\hat{s}}\right) + \log\left(\frac{\hat{u}}{\hat{s}}\right)\right] - 4\pi^2, \qquad (60)
\end{aligned}$$

where $\bar{\Delta}_{\rm UV}$ is defined in (47), and $H_1^{\rm A}(M_Z^2)$ is absent in (52). For the Abelian contributions $H_1^{\rm A}(M_V^2)$ with $V = Z, W$ we obtain

$$\begin{aligned}
g_0^{\rm A}(M_V^2) &= -\log^2\left(\frac{-\hat{s}}{M_V^2}\right) + 3\log\left(\frac{-\hat{s}}{M_V^2}\right) + \frac{3}{2}\left[\log^2\left(\frac{\hat{t}}{\hat{s}}\right) + \log^2\left(\frac{\hat{u}}{\hat{s}}\right)\right. \\
&\quad \left. + \log\left(\frac{\hat{t}}{\hat{s}}\right) + \log\left(\frac{\hat{u}}{\hat{s}}\right)\right] + \frac{7\pi^2}{3} - \frac{5}{2}, \\
g_1^{\rm A}(M_V^2) &= -g_1^{\rm N}(M_W^2) + \frac{3}{2}\left[\log\left(\frac{\hat{u}}{\hat{s}}\right) - \log\left(\frac{\hat{t}}{\hat{s}}\right)\right], \\
g_2^{\rm A}(M_V^2) &= -g_2^{\rm N}(M_W^2). \qquad (61)
\end{aligned}$$

The results (60)–(61), for the $\bar{q}q \to Zg$ process, are valid for arbitrary values of the Mandelstam invariants. They can thus be easily translated to all other processes in (2) by means of appropriate permutations of $\hat{s}, \hat{t}$ and $\hat{u}$, which are specified by the crossing relations (9) and (10). We note that the arguments of the logarithms in (60)–(61) are in general not positive. Logarithms with negative arguments are defined through the usual iε prescription, $\hat{r} \to \hat{r} + {\rm i}\varepsilon$ for $\hat{r} = \hat{s}, \hat{t}, \hat{u}$. In practice we

need only the real parts of the logarithms,

$$\begin{aligned}\text{Re}\,\log(x) &= \log(|x|),\\ \text{Re}\,\log^2(x) &= \log^2(|x|) - \pi^2\theta(-x).\end{aligned} \tag{62}$$

The π^2-terms originating from the analytic continuation of the double logarithms depend on the signs of their arguments and these latter are determined by the signs of the Mandelstam invariants. For the $\bar{q}q \to Zg$ process, one has $\hat{s} > 0, \hat{t} < 0$ and $\hat{u} < 0$. However, these signs change when the Mandelstam invariants are permuted in order to translate the results (60)–(61) for the $\bar{q}q \to Zg$ process to the other partonic processes in (2). The π^2 terms resulting from (62) are thus process dependent. Simple explicit expression that apply to all processes in (2) can be obtained using the relations

$$\theta(\hat{s}) + \theta(\hat{t}) + \theta(\hat{u}) = 1, \qquad \theta(\hat{s})\theta(\hat{t}) = \theta(\hat{t})\theta(\hat{u}) = \theta(\hat{u})\theta(\hat{s}) = 0, \tag{63}$$

which are valid for $\hat{s} > 0$, $\hat{t} < 0$ and $\hat{u} < 0$ as well as for any permutation of the Mandelstam invariants (crossing transformations). Combining (60)–(63) we obtain

$$\begin{aligned}\text{Re}\, g_0^{\text{N}}(M_W^2) &= 2\bar{\Delta}_{\text{UV}} + \log^2\left(\frac{|\hat{s}|}{M_W^2}\right) - \log^2\left(\frac{|\hat{t}|}{M_W^2}\right) - \log^2\left(\frac{|\hat{u}|}{M_W^2}\right) + \log^2\left(\frac{|\hat{t}|}{|\hat{u}|}\right)\\ &\quad - \frac{3}{2}\left[\log^2\left(\frac{|\hat{t}|}{|\hat{s}|}\right) + \log^2\left(\frac{|\hat{u}|}{|\hat{s}|}\right)\right] - \frac{\pi^2}{18}\left[4 + 9\theta(-\hat{s})\right] - \frac{2\pi}{\sqrt{3}} + 4,\\ \text{Re}\, g_1^{\text{N}}(M_W^2) &= \frac{1}{2}\left[\log^2\left(\frac{|\hat{u}|}{|\hat{s}|}\right) - \log^2\left(\frac{|\hat{t}|}{|\hat{s}|}\right)\right] + \frac{\pi^2}{2}\left[\theta(\hat{t}) - \theta(\hat{u})\right],\\ \text{Re}\, g_2^{\text{N}}(M_W^2) &= -2\left[\log^2\left(\frac{|\hat{t}|}{|\hat{s}|}\right) + \log^2\left(\frac{|\hat{u}|}{|\hat{s}|}\right) + \log\left(\frac{|\hat{t}|}{|\hat{s}|}\right) + \log\left(\frac{|\hat{u}|}{|\hat{s}|}\right)\right]\\ &\quad - 2\pi^2\theta(-\hat{s}),\end{aligned} \tag{64}$$

and

$$\begin{aligned}\text{Re}\, g_0^{\text{A}}(M_V^2) &= -\log^2\left(\frac{|\hat{s}|}{M_V^2}\right) + 3\log\left(\frac{|\hat{s}|}{M_V^2}\right) + \frac{3}{2}\left[\log^2\left(\frac{|\hat{t}|}{|\hat{s}|}\right) + \log^2\left(\frac{|\hat{u}|}{|\hat{s}|}\right)\right.\\ &\quad \left. + \log\left(\frac{|\hat{t}|}{|\hat{s}|}\right) + \log\left(\frac{|\hat{u}|}{|\hat{s}|}\right)\right] + \frac{\pi^2}{6}\left[2 + 3\theta(-\hat{s})\right] - \frac{5}{2},\\ \text{Re}\, g_1^{\text{A}}(M_V^2) &= -\text{Re}\, g_1^{\text{N}}(M_W^2) + \frac{3}{2}\left[\log\left(\frac{|\hat{u}|}{|\hat{s}|}\right) - \log\left(\frac{|\hat{t}|}{|\hat{s}|}\right)\right],\\ \text{Re}\, g_2^{\text{A}}(M_V^2) &= -\text{Re}\, g_2^{\text{N}}(M_W^2).\end{aligned} \tag{65}$$

For the $\bar{q}q \to Zg$ and $q\bar{q} \to Zg$ processes, with $\hat{s} > 0, \hat{t} < 0$ and $\hat{u} < 0$, all θ functions in (64)–(65) vanish. The θ-terms become relevant when the above results are translated to the processes that involve gluons in the initial state.

Let us compare the double and single logarithms of M_V that appear in (64)–(65) with the NLL result of Ref. [14], which is given in (57). In the $M_V^2/\hat{s} \to 0$ limit the two results agree up to contributions resulting from the difference between $g_0^{\rm A}(M_W^2)$ and $g_0^{\rm A}(M_Z^2)$. Since the calculation of Ref. [14] was based on the equal-mass approximation, $M_W = M_Z$, we conclude that the two results are consistent.

Let us now consider the contribution of the counterterms (CTs) $\delta C_{q_\lambda}^{\rm A/N}$ in (52). These CTs [see (44)–(50)] consist of on-shell gauge-boson self-energies and are independent of the high-energy scales $\hat{s}$, $\hat{t}$ and $\hat{u}$. They are thus free from large logarithms. Since the exact analytical expressions for the CTs are relatively complicated as compared to the compact NNLL contributions (64)–(65), we present simple approximate expressions for $\delta C_{q_\lambda}^{\rm A/N}$. Restricting ourselves to the case of the $\overline{\rm MS}$ scheme, we use: (i) A heavy-top expansion including terms of order $\log(m_t)$ and $(1/m_t)^0$; (ii) A first-order expansion in the Z-W mass difference, using $1 - M_W^2/M_Z^2 = s_{\rm w}^2$ as expansion parameter; (iii) The light-Higgs approximation $M_H = M_Z$. The resulting expressions for the renormalization constants associated with the Z-boson wave function read

$$\begin{aligned}
\delta\tilde{Z}_{AZ} &= \frac{\alpha}{4\pi}\frac{1}{s_{\rm w}c_{\rm w}}\bigg[-\left(\frac{7+34s_{\rm w}^2}{3}+4c_{\rm w}^2(\rho-1)\right)\bar{\Delta}_{\rm UV}-\frac{4}{9}(3-8s_{\rm w}^2)\log\left(\frac{m_t^2}{M_Z^2}\right)\\
&\quad+(17-36s_{\rm w}^2)\frac{\pi}{\sqrt{3}}-\frac{8}{27}(78-89s_{\rm w}^2)\bigg],\\
\delta\tilde{Z}_{ZZ} &= \frac{\alpha}{4\pi}\frac{1}{s_{\rm w}^2}\bigg[-\frac{5-10s_{\rm w}^2+46s_{\rm w}^4}{6c_{\rm w}^2}\bar{\Delta}_{\rm UV}+\frac{3-5s_{\rm w}^2}{6}\log\left(\frac{m_t^2}{M_Z^2}\right)\\
&\quad+\frac{11-37s_{\rm w}^2}{6}\frac{\pi}{\sqrt{3}}-\frac{113-573s_{\rm w}^2}{36}\bigg].
\end{aligned}\tag{66}$$

And for the CTs (44) within the $\overline{\rm MS}$ scheme we obtain

$$\begin{aligned}
\delta\tilde{C}_{q_\lambda}^{\rm A} &\overset{\overline{\rm MS}}{=} \frac{\alpha}{4\pi}\frac{1}{s_{\rm w}^2}\bigg[-\frac{15-49s_{\rm w}^2}{36}\log\left(\frac{m_t^2}{M_Z^2}\right)\\
&\quad+\frac{113-253s_{\rm w}^2}{12}\frac{\pi}{\sqrt{3}}-\frac{105}{8}+\frac{4567}{216}s_{\rm w}^2\bigg],\\
\delta\tilde{C}_{q_\lambda}^{\rm N} &\overset{\overline{\rm MS}}{=} -\frac{\alpha}{4\pi}\bigg\{\frac{2}{s_{\rm w}^2}\bar{\Delta}_{\rm UV}+\frac{1}{2s_{\rm w}^2c_{\rm w}^2}\bigg[-\frac{4}{9}(3-8s_{\rm w}^2)\log\left(\frac{m_t^2}{M_Z^2}\right)\\
&\quad+(17-36s_{\rm w}^2)\frac{\pi}{\sqrt{3}}-\frac{8}{27}(78-89s_{\rm w}^2)\bigg]\bigg\}.
\end{aligned}\tag{67}$$

As one can easily infer from the numerical values[7] $\delta Z_{AZ} = -2.316\times10^{-3}$, $\delta Z_{ZZ} = 3.943\times10^{-3}$, $\delta\tilde{Z}_{AZ} = -2.888\times10^{-3}$, $\delta\tilde{Z}_{ZZ} = 4.533\times10^{-3}$, the contribution of the CTs to the cross section is of order of a few permille whereas the error associated with the approximations (66),(67) is below the one permille level.

[7] These numerical values are obtained using the $\overline{\rm MS}$ input parameters given in Sect. 4 and $\bar{\Delta}_{\rm UV} = 0$.

3.6 Checks

In order to control the correctness of our results we performed various consistency checks. We have verified that the one-loop corrections (31) satisfy the Ward Identities

$$\begin{aligned}
\varepsilon_\mu^*(p_Z)\, p_{g\nu}\, \bar{v}(p_{\bar{q}}) \left[\delta\mathcal{A}^{\mu\nu}_{1,\mathrm{A/N}}(M_V^2)\omega_\lambda\right] u(p_q) &= 0, \\
p_{Z\mu}\, \varepsilon_\nu^*(p_g)\, \bar{v}(p_{\bar{q}}) \left[\delta\mathcal{A}^{\mu\nu}_{1,\mathrm{A/N}}(M_V^2)\omega_\lambda\right] u(p_q) &= 0, \\
p_{Z\mu}\, p_{g\nu}\, \bar{v}(p_{\bar{q}}) \left[\delta\mathcal{A}^{\mu\nu}_{1,\mathrm{A/N}}(M_V^2)\omega_\lambda\right] u(p_q) &= 0.
\end{aligned} \tag{68}$$

Similar Ward identities hold for the lowest-order amplitude. The cancellation of the ultraviolet divergences and the compensation of the fictitious collinear singularities discussed in Sect. 3.2 have been verified analytically and numerically. The high-energy limit of our result has been worked out analytically and we have shown that the leading- and next-to-leading logarithmic contributions agree with Ref. [14].

Moreover, the calculation has been performed in two completely independent ways, based on different computer-algebra and numerical tools. On one hand we have written algorithms for the algebraic reduction in `Mathematica` [20] and used a set of routines provided by A. Denner for the numerical evaluation of loop integrals. On the other hand we have performed the reduction by means of `FeynCalc` [17] and used `FF` [21] to evaluate loop integrals. The results have been implemented in different `Fortran` codes and comparing them we find very good agreement at numerical level.

4 Predictions for the hadronic Z production at high transverse momentum

In the following we discuss numerical predictions for the quantities calculated above. The lowest order (LO) and the next-to-leading-order (NLO) predictions result from (13) and (52)–(55), (74)–(75), respectively. The next-to-leading-logarithmic (NLL) approximation, at one loop, corresponds[8] to (57)–(58). The next-to-next-to-leading-logarithmic (NNLL) predictions, also at one loop, are based on (59)–(67). All results are obtained using LO MRST2001 parton distribution functions (PDFs) [22]. We choose p_{T}^2 as the factorization scale and, similarly as the scale at which the running strong coupling constant is evaluated. We also adopt the value $\alpha_{\mathrm{S}}(M_Z^2) = 0.13$ and use the one-loop running expression for $\alpha_{\mathrm{S}}(\mu^2)$, in accordance with the LO PDF extraction method of the MRST collaboration. We use the following values of parameters [23]: $M_Z = 91.19\,\mathrm{GeV}$, $M_W = 80.39\,\mathrm{GeV}$, $m_t = 176.9\,\mathrm{GeV}$, $m_b = 4.3\,\mathrm{GeV}$, $M_H = 120\,\mathrm{GeV}$. For the calculation in the $\overline{\mathrm{MS}}$ scheme we use $\alpha = 1/128.1$,

[8] For details concerning the treatment of angular-dependent logarithms at the NLL level we refer to Ref. [14].

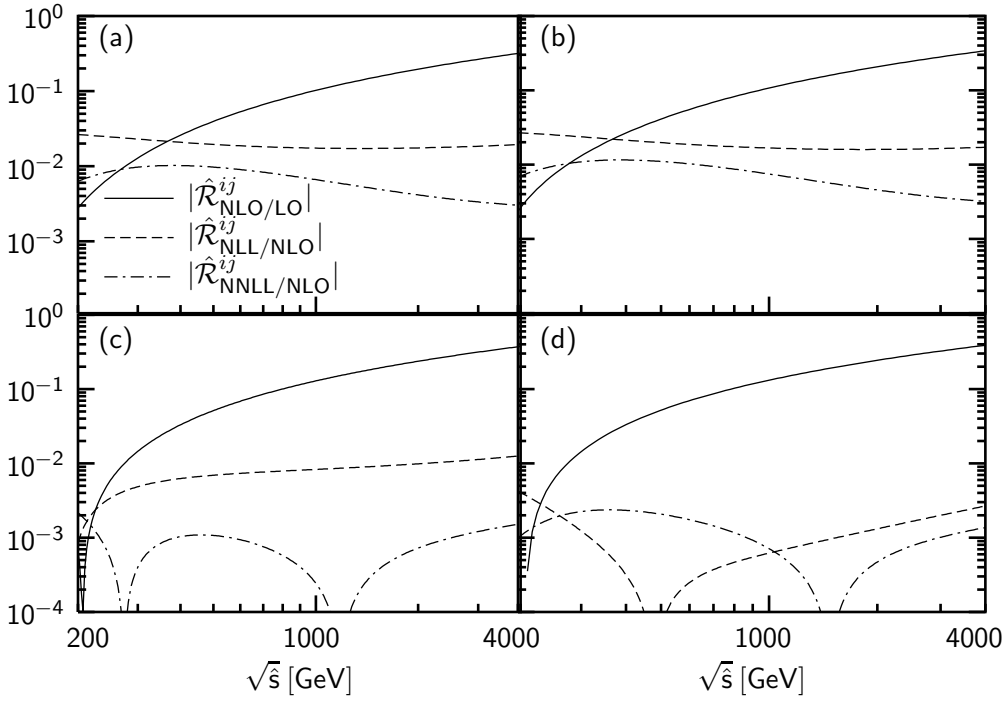

Figure 4: Relative one-loop corrections to the partonic differential cross sections $\mathrm{d}\hat{\sigma}^{ij}/\mathrm{d}\cos\theta$ at $\cos\theta = 0$ for (a) $\bar{u}u$ channel, (b) $\bar{d}d$ channel, (c) gu channel, (d) gd channel. The solid, dashed and dot-dashed lines denote the modulus of the $\hat{\mathcal{R}}$ ratios, as defined in the text, for the full NLO cross section, the NLL approximation and the NNLL approximation of the one-loop cross section, respectively.

$s^2_{\rm w} = 0.2314$, whereas for the on-shell scheme $\alpha = 1/128.9$, $s^2_{\rm w} = 1 - c^2_{\rm w} = 1 - M^2_W/M^2_Z$ are taken. The NLO predictions use the form of the counterterms given by (44)–(50), whereas the NNLL results are based on the approximate expressions (66)–(67) for the counterterms. Unless otherwise noted, the results are obtained using the $\overline{\rm MS}$ scheme.

We begin by investigating NLO, NLL and NNLL relative corrections to the partonic (unpolarized) differential cross section $\mathrm{d}\hat{\sigma}^{ij}/\mathrm{d}\cos\theta$ [see (5)]. To this end we define

$$\hat{\mathcal{R}}^{ij}_{\rm NLO/LO} = \frac{\mathrm{d}\hat{\sigma}^{ij}_{\rm NLO}/\mathrm{d}\cos\theta}{\mathrm{d}\hat{\sigma}^{ij}_{\rm LO}/\mathrm{d}\cos\theta} - 1 \tag{69}$$

and similarly $\hat{\mathcal{R}}^{ij}_{\rm NLL/NLO}$ and $\hat{\mathcal{R}}^{ij}_{\rm NNLL/NLO}$. These ratios, calculated at $\cos\theta = 0$, are displayed as a function of $\sqrt{\hat{s}}$ in Fig. 4. We consider four processes: $\bar{u}u{\to}Zg$ (Fig. 4a), $\bar{d}d{\to}Zg$ (Fig. 4b), $gu{\to}Zu$ (Fig. 4c), $gd{\to}Zd$ (Fig. 4d). The size of the full weak NLO correction grows with the energy and reaches 30% for all channels at $\sqrt{\hat{s}} = 4\,\mathrm{TeV}$. The sign of this correction is negative. From Fig. 4 we conclude that the NLL terms provide a fairly good approximation to the full NLO result for

$\sqrt{\hat{s}} \geq 200\,\mathrm{GeV}$, with the remaining terms responsible for less than 3% of the cross section in the $u\bar{u}$ and $d\bar{d}$ channels, and less than 1% in the gu and gd channels. The quality of the NNLL approximation is very good in all channels, better or comparable to 1% in the full region under consideration. The absolute LO and NLO cross section and the $\hat{\mathcal{R}}^{ij}$ ratios for specific values of $\cos\theta$, $\sqrt{\hat{s}}$ and different collision channels are listed in Table 1.

The transverse momentum distribution $\mathrm{d}\sigma/\mathrm{d}p_\mathrm{T}$ at the LHC is shown in Fig. 5. We display separately the absolute values of the LO, NLO, NLL and NNLL differential cross sections (Fig. 5a) and the relative correction wrt. the LO result for the NLO, NLL and NNLL distributions (Fig. 5b). The relative correction wrt. the LO is now defined as

$$\mathcal{R}^{\mathrm{had}}_{\mathrm{NLO/LO}} = \frac{\mathrm{d}\sigma_{\mathrm{NLO}}/\mathrm{d}p_\mathrm{T}}{\mathrm{d}\sigma_{\mathrm{LO}}/\mathrm{d}p_\mathrm{T}} - 1 \tag{70}$$

for the NLO case, and similarly for the NLL and the NNLL cross sections. The quality of the NLL and NNLL high-energy approximations is shown in more detail in Fig. 5c. The importance of the NLO corrections increases significantly with p_T. The NLO correction results in a negative contribution ranging from -13% at $p_\mathrm{T} = 500\,\mathrm{GeV}$ up to -37% at $p_\mathrm{T} = 2\,\mathrm{TeV}$ of the LO cross section. We observe that the NLL approximation works very well. It differs from the full NLO prediction by about 1% at low p_T and by 0.2% at $p_\mathrm{T} \sim 2\,\mathrm{TeV}$, cf. Fig 5c. The quality of the NNLL approximation is at the permille level (or better) in the entire p_T range.

In view of the large one-loop effects, we include the dominant two-loop terms [14]. In Fig. 6 we show the relative size of the corrections in the NLO approximation ($\mathcal{R}^{\mathrm{had}}_{\mathrm{NLO/LO}}$, solid line), and in the approximation which includes the next-to-leading logarithmic two-loop terms ($\mathcal{R}^{\mathrm{had}}_{\mathrm{NNLO/LO}}$, dotted line). These additional two-loop terms are positive and amount to 8% for $p_\mathrm{T} = 2\,\mathrm{TeV}$.

To underline the relevance of these effects, in Fig. 7 we present the relative NLO and NNLO corrections for the cross section, integrated over p_T starting from $p_\mathrm{T} = p_\mathrm{T}^{\mathrm{cut}}$, as a function of $p_\mathrm{T}^{\mathrm{cut}}$. This is compared with the statistical error, defined as $\Delta\sigma_{\mathrm{stat}}/\sigma = 1/\sqrt{N}$ with $N = \mathcal{L} \times \mathrm{BR}(Z{\to}l,\nu_l) \times \sigma_{\mathrm{LO}}$. We include all leptonic decay modes of Z, corresponding to BR = 30.6%, and assume a total integrated luminosity $\mathcal{L} = 300\,\mathrm{fb}^{-1}$ for the LHC [24]. It is clear from Fig. 7, that the size of the one- and two-loop corrections is much bigger than and comparable to the statistical error, respectively.

We also perform a similar analysis for high transverse momentum Z production at the Tevatron. In Fig. 8 we show the transverse momentum distribution (Fig. 8a), the relative size of the corrections (Fig. 8b) and the quality of the one-loop NLL and NNLL approximations (Fig. 8c). In Fig. 9 the relative size of the corrections to the integrated cross section is compared with the statistical error expected for an integrated luminosity $\mathcal{L} = 11\,\mathrm{fb}^{-1}$ [25]. At the energies of the Fermilab collider, the NLO weak correction is of the order of the statistical error and should be taken into account when considering precision measurements. The two-loop terms turn out to be negligible.

			$\mathrm{d}\hat{\sigma}^{ij}/\mathrm{d}\cos\theta$ [pb]		$\hat{\mathcal{R}}^{ij}_{\mathrm{A/B}} \times 10^3$		
ij	$\frac{\sqrt{\hat{s}}}{\mathrm{GeV}}$	$\cos\theta$	LO	NLO	NLO/LO	NLL/NLO	NNLL/NLO
$\bar{u}u$	500	0.0	1.7012×10^{0}	1.6341×10^{0}	−39.431	19.501	9.7186
	1000	0.0	3.5934×10^{-1}	3.2261×10^{-1}	−102.22	17.397	6.6197
	2000	0.0	8.1081×10^{-2}	6.5185×10^{-2}	−196.05	17.518	4.1422
$\bar{u}u$	500	0.5	2.8203×10^{0}	2.7210×10^{0}	−35.224	25.906	7.2284
	1000	0.5	6.0587×10^{-1}	5.4862×10^{-1}	−94.497	24.664	4.9420
	2000	0.5	1.3718×10^{-1}	1.1185×10^{-1}	−184.66	25.881	3.2372
$\bar{d}d$	500	0.0	2.1930×10^{0}	2.1031×10^{0}	−40.978	19.759	11.038
	1000	0.0	4.6322×10^{-1}	4.1349×10^{-1}	−107.36	16.723	7.4723
	2000	0.0	1.0452×10^{-1}	8.2852×10^{-2}	−207.31	16.002	4.5613
$\bar{d}d$	500	0.5	3.6357×10^{0}	3.5013×10^{0}	−36.970	25.829	8.3255
	1000	0.5	7.8103×10^{-1}	7.0278×10^{-1}	−100.18	23.838	5.6448
	2000	0.5	1.7684×10^{-1}	1.4205×10^{-1}	−196.74	24.376	3.5721
gu	500	0.0	6.9404×10^{-1}	6.5844×10^{-1}	−51.284	−6.9286	−1.0724
	1000	0.0	1.6267×10^{-1}	1.4171×10^{-1}	−128.83	−8.2907	−0.2447
	2000	0.0	3.7676×10^{-2}	2.8750×10^{-2}	−236.92	−9.8681	0.7254
gu	500	0.5	5.9307×10^{-1}	5.5148×10^{-1}	−70.127	−13.649	0.9367
	1000	0.5	1.3822×10^{-1}	1.1654×10^{-1}	−156.82	−16.198	1.0469
	2000	0.5	3.1936×10^{-2}	2.3182×10^{-2}	−274.09	−19.650	1.4449
gd	500	0.0	8.9468×10^{-1}	8.4822×10^{-1}	−51.931	−0.0567	−2.0723
	1000	0.0	2.0969×10^{-1}	1.8206×10^{-1}	−131.76	−0.6210	−0.7120
	2000	0.0	4.8569×10^{-2}	3.6717×10^{-2}	−244.01	−1.3163	0.4704
gd	500	0.5	7.6453×10^{-1}	7.1421×10^{-1}	−65.819	−5.1329	−0.1256
	1000	0.5	1.7818×10^{-1}	1.5103×10^{-1}	−152.38	−6.6209	0.5373
	2000	0.5	4.1168×10^{-2}	2.9994×10^{-2}	−271.41	−8.7165	1.1609

Table 1: Absolute value of the LO and NLO partonic differential cross section $\mathrm{d}\hat{\sigma}^{ij}/\mathrm{d}\cos\theta$ and the ratios $\hat{\mathcal{R}}^{ij}_{\mathrm{NLO/LO}}$, $\hat{\mathcal{R}}^{ij}_{\mathrm{NLL/NLO}}$ and $\hat{\mathcal{R}}^{ij}_{\mathrm{NNLL/NLO}}$ in permille, for the partonic processes $\bar{u}u \to Zg$, $\bar{d}d \to Zg$, $gu \to Zu$ and $gd \to Zd$. The running strong coupling $\alpha_{\mathrm{S}}(\mu^2)$ is taken at the scale $\mu^2 = p_{\mathrm{T}}^2 = (1-\cos^2\theta)(1 - M_Z^2/\hat{s})^2\hat{s}/4$.

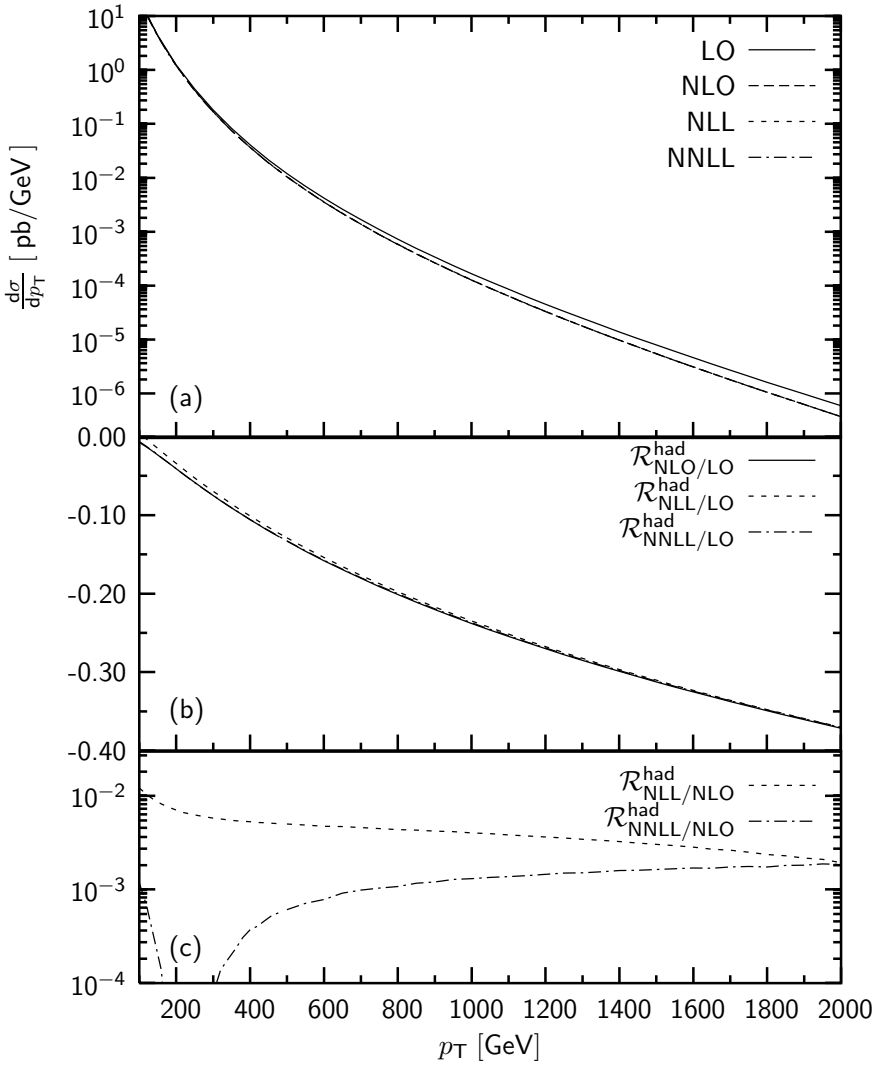

Figure 5: Transverse momentum distribution for $pp \to Zj$ at $\sqrt{s} = 14\,\text{TeV}$. (a) LO (solid), NLO (dashed), NLL (dotted) and NNLL (dot-dashed) predictions. (b) Relative NLO (solid), NLL (dotted) and NNLL (dot-dashed) weak correction wrt. the LO distribution. (c) NLL (dotted) and NNLL (dot-dashed) approximations compared to the full NLO result.

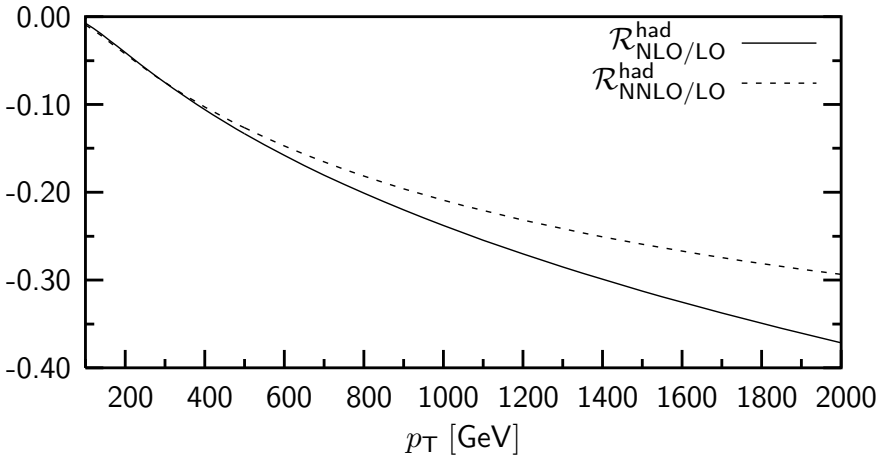

Figure 6: Relative NLO (solid) and NNLO (dotted) corrections to the p_T distribution for $pp \to Zj$ at $\sqrt{s} = 14\,\text{TeV}$.

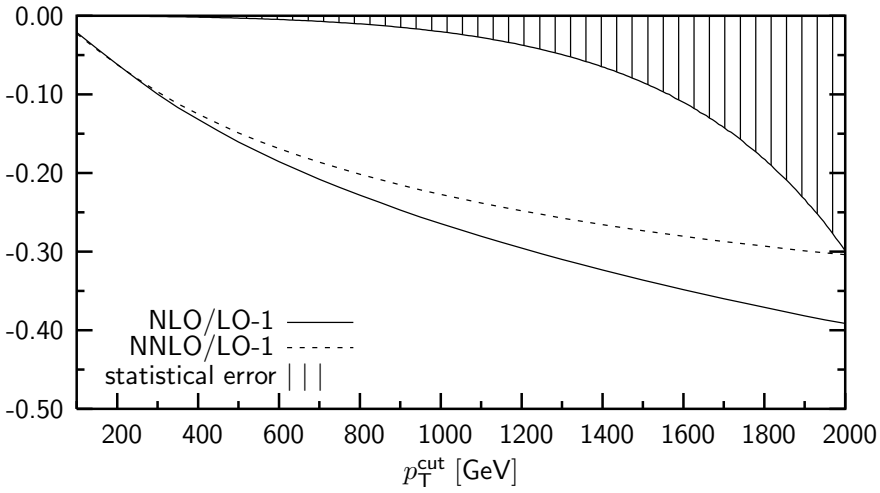

Figure 7: Relative NLO (solid) and NNLO (dotted) corrections wrt. the LO prediction and statistical error (shaded area) for the unpolarized integrated cross section for $pp \to Zj$ at $\sqrt{s} = 14\,\text{TeV}$ as a function of p_T^{cut}.

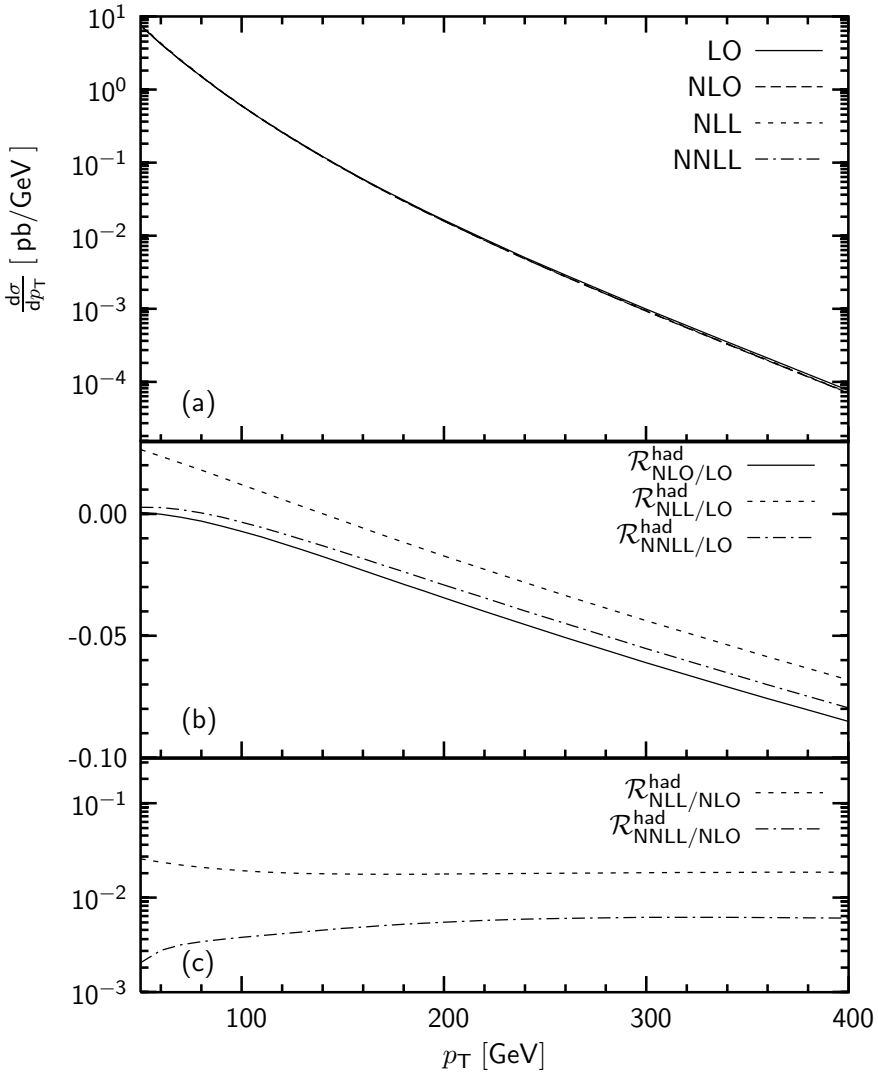

Figure 8: Transverse momentum distribution for $p\bar{p}\to Zj$ at $\sqrt{s} = 2\,\text{TeV}$. (a) LO (solid), NLO (dashed), NLL (dotted) and NNLL (dot-dashed) predictions. (b) Relative NLO (solid), NLL (dotted) and NNLL (dot-dashed) weak correction wrt. the LO distribution. (c) NLL (dotted) and NNLL (dot-dashed) approximations compared to the full NLO result.

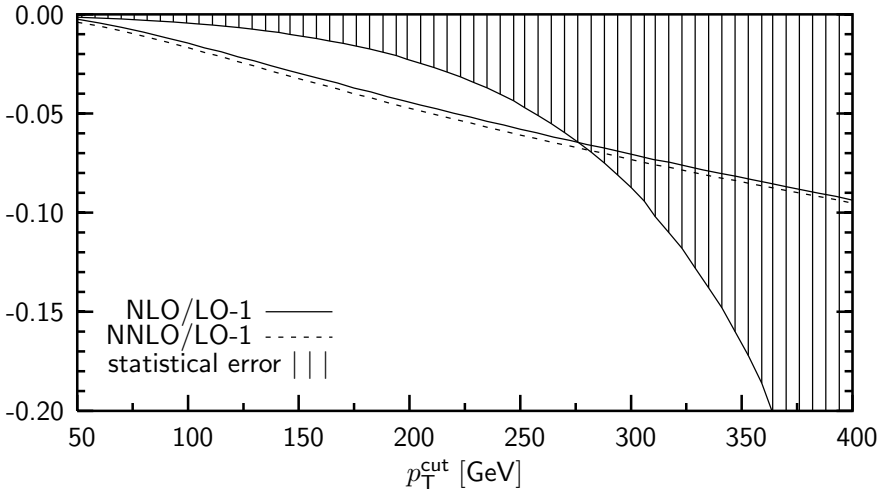

Figure 9: Relative NLO (solid) and NNLO (dotted) corrections wrt. the LO and statistical error (shaded area) for the unpolarized integrated cross section for $p\bar{p}\to Zj$ at $\sqrt{s} = 2\,\mathrm{TeV}$ as a function of $p_\mathrm{T}^\mathrm{cut}$.

Finally, in Fig. 10 we illustrate the dependence of the NLO p_T distribution on the choice of the renormalization scheme. At low p_T the results in the on-shell and $\overline{\mathrm{MS}}$ schemes differ by around 1% and the difference grows with p_T reaching 6% at $p_\mathrm{T} = 2\,\mathrm{TeV}$. This effect is mainly due to the different treatment of the weak mixing angle in the two renormalization schemes. As well known, the relation between the $\overline{\mathrm{MS}}$ and on-shell definitions of the weak mixing angle is provided by the ρ parameter as [26]

$$\frac{c_\mathrm{w}^2}{\hat{c}_\mathrm{w}^2} = \frac{M_W^2}{M_Z^2\,\hat{c}_\mathrm{w}^2} = \rho, \qquad \frac{\hat{s}_\mathrm{w}^2}{s_\mathrm{w}^2} - 1 = \Delta s_\mathrm{w}^2 = \frac{c_\mathrm{w}^2}{s_\mathrm{w}^2}\Delta\rho, \tag{71}$$

where $\rho = (1-\Delta\rho)^{-1}$ and the symbols with and without hat denote $\overline{\mathrm{MS}}$ and on-shell quantities, respectively. The input parameters used in our calculation, $\hat{s}_\mathrm{w}^2 = 0.2314$ and $s_\mathrm{w}^2 = 1 - M_W^2/M_Z^2 \simeq 0.2228$, correspond to $\Delta s_\mathrm{w}^2 \simeq 3.8\%$ and are extracted from precision electroweak measurements taking all available loop corrections into account. Instead, loop corrections beyond $\mathcal{O}(\alpha)$ are not included in our calculation and, in particular, the deviation observed in Fig. 10 is due to missing two-loop (and higher-order) corrections related to the ρ parameter. The scheme dependence resulting from α/s_w^2 terms amounts to

$$\frac{\alpha}{s_\mathrm{w}^2}(1 - \Delta^{(1)}s_\mathrm{w}^2) - \frac{\alpha}{\hat{s}_\mathrm{w}^2} \simeq \frac{\alpha}{\hat{s}_\mathrm{w}^2}(\Delta s_\mathrm{w}^2 - \Delta^{(1)}s_\mathrm{w}^2), \tag{72}$$

where $\Delta^{(1)}s_\mathrm{w}^2 = (c_\mathrm{w}^2/s_\mathrm{w}^2)\Delta\rho^{(1)} \simeq 4.5\%$ corresponds to the one-loop corrections to the ρ parameter, which are included in our on-shell predictions through the counterterm (48). This scheme dependence (72) is thus due to the higher-order contributions $\Delta s_\mathrm{w}^2 - \Delta^{(1)}s_\mathrm{w}^2 \simeq -0.7\%$. Their relatively large size results from the combined effect

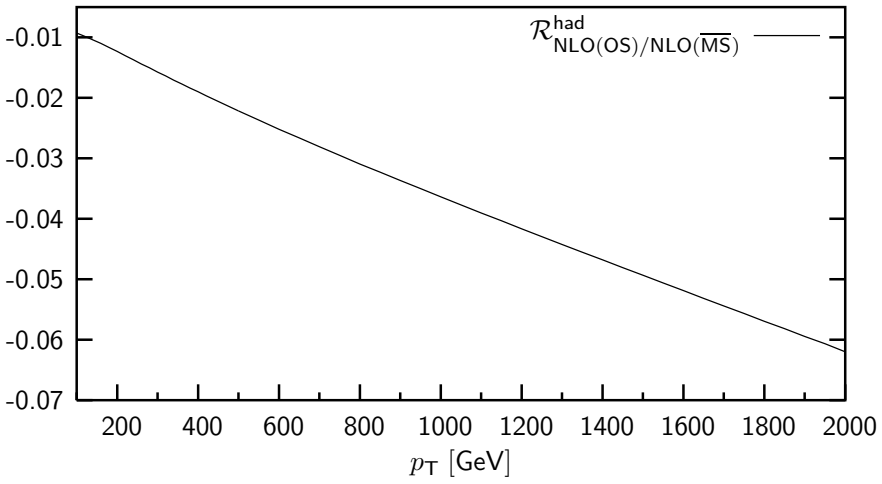

Figure 10: Relative difference of the NLO transverse momentum distribution for $pp \to Zj$ calculated in the $\overline{\rm MS}$ and on-shell (OS) schemes at $\sqrt{s} = 14\,\text{TeV}$.

of $\mathcal{O}(\alpha\alpha_{\rm S} m_t^2)$ [27], $\mathcal{O}(\alpha\alpha_{\rm S}^2 m_t^2)$ [28], $\mathcal{O}(\alpha^2 m_t^4)$ [29] and $\mathcal{O}(\alpha^2 m_t^2)$ [30] corrections to the ρ parameter and is consistent with the effect observed in Fig. 10 at small $p_{\rm T}$. In addition, the scheme-dependence resulting from the one-loop logarithmic terms is of order

$$-\left(\frac{\alpha^2}{s_{\rm w}^4} - \frac{\alpha^2}{\hat{s}_{\rm w}^4}\right) \log^2(\hat{s}/M_W^2) \simeq -2\Delta s_{\rm w}^2 \frac{\alpha^2}{s_{\rm w}^4} \log^2(\hat{s}/M_W^2). \tag{73}$$

This effect is due to missing two-loop corrections of order $\Delta\rho\,\alpha\log^2(\hat{s}/M_W^2)$. Its size is proportional to $\Delta s_{\rm w}^2 \simeq 3.8\%$ and grows with energy. This explains the high-$p_{\rm T}$ behaviour in Fig. 10.

We stress that the effects (72)–(73) are entirely due to missing higher-order terms related to $\Delta\rho$ and that such missing terms concern only the calculation in the on-shell scheme. Indeed, $\Delta\rho$ enters our predictions only through the relation between the weak mixing angle and the weak-boson masses in the on-shell scheme whereas the $\overline{\rm MS}$ calculation does not receive any contribution from $\Delta\rho$. The large scheme-dependence in Fig. 10 has thus to be interpreted as large uncertainty of the one-loop prediction in the on-shell scheme whereas such uncertainties are absent in the $\overline{\rm MS}$ scheme. This motivates the choice of the $\overline{\rm MS}$ scheme adopted in this paper.

5 Summary

In this work we have calculated the one-loop weak corrections to hadronic production of Z bosons at large transverse momenta. Analytical results are presented for the parton subprocess $\bar{q}q \to Zg$ and its crossed versions. Special attention has been devoted to the high-energy region, $\hat{s} \gg M_W^2$, where the weak corrections are enhanced

by logarithms of $\hat{s}/M_W^2$. For this region we have derived approximate expressions that include all large logarithms as well as those terms that are not logarithmically enhanced. The quadratic and linear logarithms confirm earlier results obtained to next-to-leading logarithmic accuracy. The complete high-energy approximation presented in this paper is in excellent agreement with the exact one-loop predictions. We give numerical results for proton-antiproton collisions at 2 TeV (Tevatron) and proton-proton collisions at 14 TeV (LHC) in the region of large tranverse momentum (p_{T}). The corrections are negative and their size increases with p_{T}. At the Tevatron, transverse momenta up to 300 GeV will be explored and the weak corrections may reach up to -7%. At the LHC, transverse momenta of 2 TeV or more are within the reach. In this region the corrections are large, -30% up to -40%, and even the dominant two-loop logarithmic terms must be included in any realistic prediction.

A Analytical results

Here we present the explicit analytical expressions for the coefficients $K_j^{\mathrm{A/N}}(M_V^2)$, which are defined in (56) and correspond to the Abelian (A) and non-Abelian (N) contributions resulting from the Feynman diagrams of Fig. 2.

Abelian coefficients

$$
\begin{aligned}
K_0^{\mathrm{A}}(M_V^2) &= -\frac{4\hat{s}^2+3(\hat{t}^2+\hat{u}^2)}{\hat{t}\hat{u}} + \hat{s}\left(\frac{1}{\hat{s}+\hat{t}}+\frac{1}{\hat{s}+\hat{u}}-\frac{5}{\hat{u}}-\frac{5}{\hat{t}}+\frac{4}{\hat{t}+\hat{u}}\right),\\
K_1^{\mathrm{A}}(M_V^2) &= -\left[\frac{3\hat{s}}{(\hat{s}+\hat{t})^2}+\frac{3\hat{s}}{(\hat{s}+\hat{u})^2}\right]+\left(\frac{1}{\hat{s}+\hat{t}}+\frac{1}{\hat{s}+\hat{u}}\right)-2\left(\frac{\hat{s}+\hat{u}}{\hat{t}^2}+\frac{\hat{s}+\hat{t}}{\hat{u}^2}\right)\\
&\quad+\frac{2\hat{s}^2(2\hat{s}+\hat{t}+\hat{u})}{\hat{t}\hat{u}(\hat{s}+\hat{t})(\hat{s}+\hat{u})}+4\frac{(\hat{s}+\hat{t})^2+(\hat{s}+\hat{u})^2}{\hat{t}\hat{u}M_V^2},\\
K_2^{\mathrm{A}}(M_V^2) &= M_Z^2\left[\frac{6\hat{s}M_V^2}{(\hat{s}+\hat{t})^3}+\frac{6\hat{s}M_V^2}{(\hat{s}+\hat{u})^3}+\frac{2\hat{s}M_V^2}{(\hat{s}+\hat{t})^2\hat{u}}+\frac{2\hat{s}M_V^2}{(\hat{s}+\hat{u})^2\hat{t}}+\frac{4(\hat{s}+\hat{t}+\hat{u})}{(\hat{t}+\hat{u})^2}-\frac{3}{\hat{t}}\right.\\
&\quad\left.-\frac{3}{\hat{u}}+\frac{2\hat{s}+\hat{t}-2M_V^2}{(\hat{s}+\hat{t})^2}+\frac{2\hat{s}+\hat{u}-2M_V^2}{(\hat{s}+\hat{u})^2}-\frac{\hat{s}(2\hat{s}+\hat{t}+\hat{u})(2M_V^2+3\hat{s})}{\hat{t}\hat{u}(\hat{s}+\hat{t})(\hat{s}+\hat{u})}\right],\\
K_3^{\mathrm{A}}(M_V^2) &= 0,\\
K_4^{\mathrm{A}}(M_V^2) &= -\frac{4\hat{s}(\hat{s}+2\hat{t}+2\hat{u})}{(\hat{t}+\hat{u})^2},\\
K_5^{\mathrm{A}}(M_V^2) &= -\frac{6M_V^2\hat{s}\hat{u}}{(\hat{s}+\hat{t})^3}+\frac{M_V^2(2\hat{u}-5\hat{s})-\hat{s}\hat{u}}{(\hat{s}+\hat{t})^2}+\frac{2M_V^2(\hat{s}+\hat{t}+\hat{u})}{\hat{u}^2}-\frac{M_V^2+4\hat{s}+\hat{u}}{\hat{s}+\hat{t}},\\
K_6^{\mathrm{A}}(M_V^2) &= K_5^{\mathrm{A}}(M_V^2)\Big|_{\hat{t}\leftrightarrow\hat{u}},
\end{aligned}
$$

$$
\begin{aligned}
K_7^{\rm A}(M_V^2) &= -\frac{\hat{s}}{\hat{t}\hat{u}}\Big[2(\hat{s}+M_V^2)(\hat{t}+\hat{u})+\hat{t}^2+\hat{u}^2\Big],\\
K_8^{\rm A}(M_V^2) &= \frac{M_Z^2M_V^2}{\hat{u}(\hat{u}-M_Z^2)^3}\Big[2\hat{t}M_V^2(\hat{u}-\hat{s}-\hat{t})-4M_Z^2\hat{s}(\hat{s}+\hat{t}+M_V^2)\Big],\\
K_9^{\rm A}(M_V^2) &= 0,\\
K_{10}^{\rm A}(M_V^2) &= K_8^{\rm A}(M_V^2)\Big|_{\hat{t}\leftrightarrow\hat{u}},\\
K_{11}^{\rm A}(M_V^2) &= 0,\\
K_{12}^{\rm A}(M_V^2) &= -\frac{M_V^2(\hat{t}+\hat{u})+\hat{s}\hat{u}}{\hat{t}\hat{u}}\Big[2(\hat{s}+M_V^2)(\hat{s}+M_V^2+\hat{t})+\hat{t}^2\Big],\\
K_{13}^{\rm A}(M_V^2) &= K_{12}^{\rm A}(M_V^2)\Big|_{\hat{t}\leftrightarrow\hat{u}},\\
K_{14}^{\rm A}(M_V^2) &= 0.
\end{aligned}
\tag{74}
$$

Non-Abelian coefficients

$$
\begin{aligned}
K_0^{\rm N}(M_W^2) &= \frac{4\hat{s}}{\hat{t}\hat{u}}(\hat{s}+\hat{t}+\hat{u})-2\hat{s}\left(\frac{1}{\hat{s}+\hat{u}}+\frac{1}{\hat{s}+\hat{t}}+\frac{2}{\hat{t}+\hat{u}}\right)+2\left(\frac{\hat{t}}{\hat{u}}+\frac{\hat{u}}{\hat{t}}\right),\\
K_1^{\rm N}(M_W^2) &= 0,\\
K_2^{\rm N}(M_W^2) &= -K_2^{\rm A}(M_W^2),\\
K_3^{\rm N}(M_W^2) &= 2M_W^2\left[\frac{3\hat{s}\hat{t}}{(\hat{s}+\hat{u})^3}+\frac{3\hat{s}\hat{u}}{(\hat{s}+\hat{t})^3}\right]-\frac{1}{\hat{t}\hat{u}}\left[\frac{1}{(\hat{s}+\hat{t})^2}+\frac{1}{(\hat{s}+\hat{u})^2}\right]\Big\{\hat{s}^4-2\hat{t}^2\hat{u}^2\\
&\quad+\hat{s}^2(\hat{t}+\hat{u})(2\hat{s}+\hat{t}+\hat{u})+2M_W^2\Big[\hat{s}^2(\hat{s}+\hat{t}+\hat{u})-\hat{t}\hat{u}(2\hat{s}-\hat{t}-\hat{u})\Big]\Big\},\\
K_4^{\rm N}(M_W^2) &= -K_4^{\rm A}(M_W^2),\\
K_5^{\rm N}(M_W^2) &= \frac{2\hat{s}(\hat{s}+\hat{t})-2\hat{t}\hat{u}}{(\hat{s}+\hat{t})^2},\\
K_6^{\rm N}(M_W^2) &= K_5^{\rm N}(M_W^2)\Big|_{\hat{t}\leftrightarrow\hat{u}},\\
K_7^{\rm N}(M_W^2) &= -K_7^{\rm A}(M_W^2),\\
K_8^{\rm N}(M_W^2) &= -K_8^{\rm A}(M_W^2),\\
K_9^{\rm N}(M_W^2) &= 2\hat{u}-\frac{\hat{s}^2-\hat{s}\hat{t}}{\hat{t}}+\frac{\hat{s}^2+\hat{s}\hat{t}}{\hat{u}}+2M_W^2\left[\frac{2\hat{s}^2+\hat{t}\hat{s}+\hat{t}^2}{\hat{t}\hat{u}}-\frac{2\hat{t}\hat{u}}{(\hat{s}+\hat{t})^2}-\frac{\hat{t}-\hat{s}}{\hat{t}}\right]\\
&\quad+\frac{2M_W^4}{\hat{s}+\hat{t}}\left[\frac{\hat{s}^2}{\hat{t}\hat{u}}-\frac{\hat{u}(2\hat{s}-\hat{t})}{(\hat{s}+\hat{t})^2}-\frac{4\hat{s}}{\hat{s}+\hat{t}}\right],\\
K_{10}^{\rm N}(M_W^2) &= K_8^{\rm N}(M_W^2)\Big|_{\hat{t}\leftrightarrow\hat{u}} = -K_{10}^{\rm A}(M_W^2),\\
K_{11}^{\rm N}(M_W^2) &= K_9^{\rm N}(M_W^2)\Big|_{\hat{t}\leftrightarrow\hat{u}},\\
K_{12}^{\rm N}(M_W^2) &= -K_{12}^{\rm A}(M_W^2),
\end{aligned}
$$

$$K_{13}^{\rm N}(M_W^2) = K_{12}^{\rm N}(M_W^2)\Big|_{\hat{t}\leftrightarrow\hat{u}} = -K_{13}^{\rm A}(M_W^2),$$
$$K_{14}^{\rm N}(M_W^2) = \frac{M_W^2(\hat{t}+\hat{u})-\hat{t}\hat{u}}{\hat{t}\hat{u}}\Bigg[2M_W^4 + 2(2\hat{s}+\hat{t}+\hat{u})M_W^2 - 2\hat{t}\hat{u} - \hat{s}(\hat{t}+\hat{u})\Bigg]. \quad (75)$$

Acknowledgements

S. P. is grateful to A. Denner for providing a set of routines for the numerical evaluation of one-loop integrals. This work was supported in part by BMBF Grant No. 05HT4VKA/3 and by the Deutsche Forschungsgemeinschaft (Sonderforschungsbereich Transregio SFB/TR-9 "Computational Particle Physics"). M. S. would like to acknowledge financial support from the Graduiertenkolleg "Hochenergiephysik und Teilchenastrophysik".

References

[1] G. Arnison *et al.* [UA1 Collaboration], Phys. Lett. B **122** (1983) 103; Phys. Lett. B **126** (1983) 398;
M. Banner *et al.* [UA2 Collaboration], Phys. Lett. B **122** (1983) 476;
P. Bagnaia *et al.* [UA2 Collaboration], Phys. Lett. B **129** (1983) 130.

[2] S. Catani *et al.*, hep-ph/0005025.

[3] Yu. L. Dokshitzer, D. I. D'Yakonov, and S. I. Troyan, Phys. Lett. B **79** (1978) 269;
G. Parisi and R. Petronzio, Nucl. Phys. B **154** (1979) 427;
G. Altarelli, R. K. Ellis, M. Greco and G. Martinelli, Nucl. Phys. B **246** (1984) 12;
J. C. Collins and D. E. Soper, Nucl. Phys. B **193** (1981) 381 [Erratum-ibid. B **213** (1983) 545]; Nucl. Phys. B **197** (1982) 446;
J. C. Collins, D. E. Soper and G. Sterman, Nucl. Phys. B **250** (1985) 199;
C. T. H. Davies and W. J. Stirling, Nucl. Phys. B **244** (1984) 337;
C. T. H. Davies, B. R. Webber and W. J. Stirling, Nucl. Phys. B **256** (1985) 413;
P. B. Arnold and R. P. Kauffman, Nucl. Phys. B **349** (1991) 381.

[4] C. Balázs and C. P. Yuan, Phys. Rev. D **56** (1997) 5558 [hep-ph/9704258];
R. K. Ellis and S. Veseli, Nucl. Phys. B **511** (1998) 649 [hep-ph/9706526];
A. Kulesza and W. J. Stirling, Nucl. Phys. B **555** (1999) 279 [hep-ph/9902234];
Eur. Phys. J. C **20** (2001) 349 [hep-ph/0103089];
J.-W. Qiu and X.-F. Zhang Phys. Rev. Lett. **86** (2001) 2724 [hep-ph/0012058];
Phys. Rev. D **63** (2001) 114011 [hep-ph/0012348];
A. Kulesza, G. Sterman and W. Vogelsang, Phys. Rev. D **66** (2002) 014011 [hep-ph/0202251].

[5] R. K. Ellis, G. Martinelli and R. Petronzio, Nucl. Phys. B **211** (1983) 106;
P. B. Arnold and M. H. Reno, Nucl. Phys. B **319** (1989) 37 [Erratum-ibid. B **330** (1990) 284];
R. J. Gonsalves, J. Pawlowski and C. F. Wai, Phys. Rev. D **40** (1989) 2245;
W. T. Giele, E. W. N. Glover and D. A. Kosower, Nucl. Phys. B **403** (1993) 633 [hep-ph/9302225];
J. Campbell and R. K. Ellis, Phys. Rev. D **65** (2002) 113007 [hep-ph/0202176];
J. Campbell, R. K. Ellis and D. L. Rainwater, Phys. Rev. D **68** (2003) 094021 [hep-ph/0308195].

[6] A. Gehrmann-De Ridder, T. Gehrmann and E. W. N. Glover, Nucl. Phys. Proc. Suppl. **135** (2004) 97 [hep-ph/0407023];
S. Weinzierl, hep-ph/0408278.

[7] J. H. Kühn and A. A. Penin, hep-ph/9906545;
J. H. Kühn, A. A. Penin and V. A. Smirnov, Eur. Phys. J. C **17** (2000) 97 [hep-ph/9912503];
J. H. Kühn *et al.*, Nucl. Phys. B **616** (2001) 286 [hep-ph/0106298];
B. Feucht, J. H. Kühn and S. Moch, Phys. Lett. B **561** (2003) 111 [hep-ph/0303016];
B. Feucht *et al.*, Phys. Rev. Lett. **93** (2004) 101802 [hep-ph/0404082];
B. Jantzen *et al.*, hep-ph/0504111.

[8] S. Pozzorini, Nucl. Phys. B **692** (2004) 135 [hep-ph/0401087].

[9] A. Denner and S. Pozzorini, Eur. Phys. J. C **18** (2001) 461 [hep-ph/0010201]; Eur. Phys. J. C **21** (2001) 63 [hep-ph/0104127].

[10] S. Pozzorini, *doctoral thesis, Universität Zürich, 2001*, hep-ph/0201077.

[11] A. Denner, M. Melles and S. Pozzorini, Nucl. Phys. B **662** (2003) 299 [hep-ph/0301241].

[12] W. Hollik *et al.*, Acta Phys. Polon. B **35** (2004) 2533 [hep-ph/0501246].

[13] E. Accomando, A. Denner and S. Pozzorini, Phys. Rev. D **65** (2002) 073003 [hep-ph/0110114];
W. Hollik and C. Meier, Phys. Lett. B **590** (2004) 69 [hep-ph/0402281];
E. Accomando, A. Denner and A. Kaiser, Nucl. Phys. B **706** (2005) 325 [hep-ph/0409247];
S. Moretti, M. R. Nolten and D. A. Ross, hep-ph/0503152.

[14] J. H. Kühn, A. Kulesza, S. Pozzorini and M. Schulze, Phys. Lett. B **609** (2005) 277 [hep-ph/0408308].

[15] E. Maina, S. Moretti and D. A. Ross, Phys. Lett. B **593** (2004) 143 [Erratum-ibid. B **614** (2005) 216] [hep-ph/0403050].

[16] A. Denner, Fortsch. Phys. **41** (1993) 307.

[17] R. Mertig, M. Bohm and A. Denner, Comput. Phys. Commun. **64** (1991) 345; http://www.feyncalc.org/.

[18] S. Dittmaier, Nucl. Phys. B **675** (2003) 447 [hep-ph/0308246].

[19] M. Roth and A. Denner, Nucl. Phys. B **479** (1996) 495 [hep-ph/9605420].

[20] Wolfram Research, Inc., Mathematica, Version 4.2, Champaign, IL (2002).

[21] G. J. van Oldenborgh, Comput. Phys. Commun. **66** (1991) 1.

[22] A. D. Martin, R. G. Roberts, W. J. Stirling and R. S. Thorne, Phys. Lett. B **531** (2002) 216 [hep-ph/0201127].

[23] S. Eidelman *et al.* [Particle Data Group], Phys. Lett. B **592** (2004) 1.

[24] V. A. Mitsou, hep-ph/0004161.

[25] Department of Energy Review Committee Report on the Run II Luminosity Performance of the Fermilab Tevatron, October 28-31 2002, http://www-bd.fnal.gov/doereview02/Run_II_lum_review_Final.pdf

[26] G. Degrassi, S. Fanchiotti and A. Sirlin, Nucl. Phys. B **351** (1991) 49.

[27] A. Djouadi and C. Verzegnassi, Phys. Lett. B **195** (1987) 265;
B. A. Kniehl, Nucl. Phys. B **347** (1990) 86.

[28] K. G. Chetyrkin, J. H. Kühn and M. Steinhauser, Phys. Lett. B **351** (1995) 331 [hep-ph/9502291].

[29] R. Barbieri, M. Beccaria, P. Ciafaloni, G. Curci and A. Vicere, Phys. Lett. B **288** (1992) 95 [Erratum-ibid. B **312** (1993) 511] [hep-ph/9205238];
R. Barbieri, M. Beccaria, P. Ciafaloni, G. Curci and A. Vicere, Nucl. Phys. B **409** (1993) 105;
J. Fleischer, O. V. Tarasov and F. Jegerlehner, Phys. Lett. B **319** (1993) 249;
G. Degrassi, S. Fanchiotti and P. Gambino, Int. J. Mod. Phys. A **10** (1995) 1377 [hep-ph/9403250].

[30] G. Degrassi, P. Gambino and A. Vicini, Phys. Lett. B **383** (1996) 219 [hep-ph/9603374];
G. Degrassi, P. Gambino and A. Sirlin, Phys. Lett. B **394** (1997) 188 [hep-ph/9611363].